Lawrence Berkeley Laboratory
UNIVERSITY OF CALIFORNIA

Materials & Molecular Research Division

NUCLEAR MATERIALS RESEARCH PROGRESS REPORTS FOR 1977

D. R. Olander

December 1977

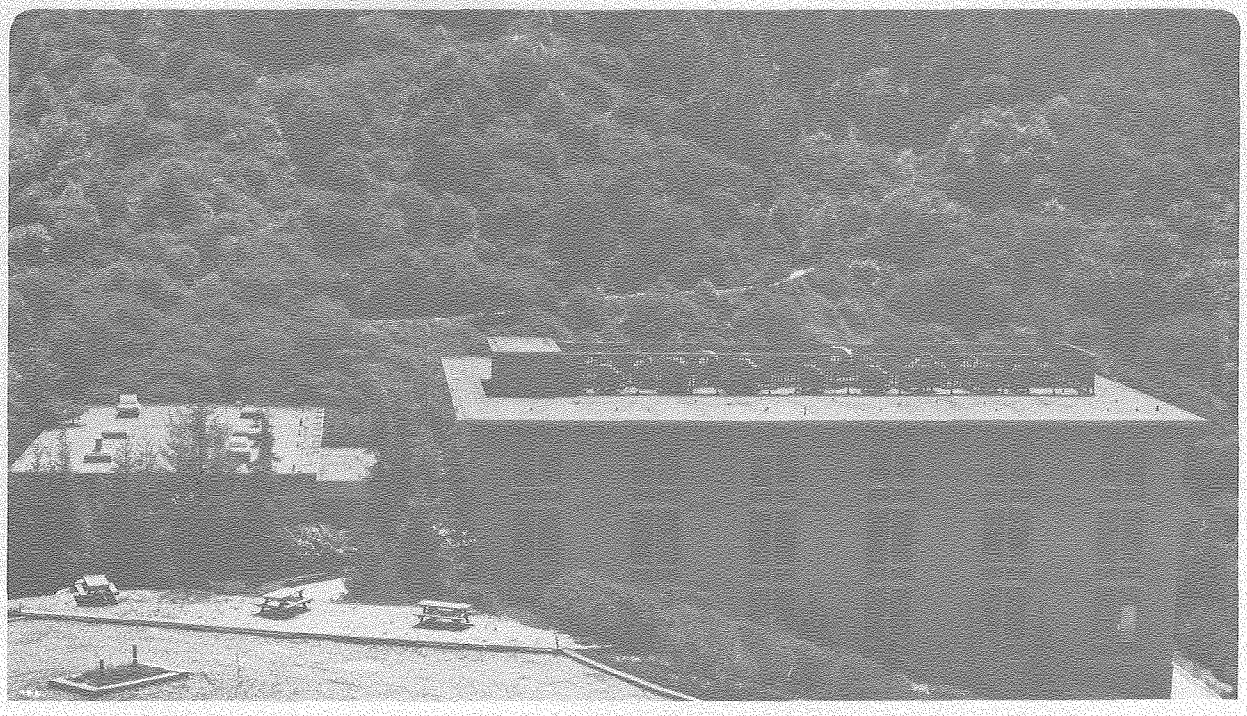

Prepared for the U.S. Department of Energy under Contract W-7405-ENG-48

DISCLAIMER

LBL-10374

NUCLEAR MATERIALS RESEARCH PROGRESS REPORTS

FOR 1977

Materials and Molecular Research Division
Lawrence Berkeley Laboratory
University of California
Berkeley, California 94720

D. R. Olander,

Principal Investigator

This work was supported by the U. S. Department of Energy under Contract W-7405-ENG-48

CONTENTS

RADIATION ENHANCEMENT OF STRESS CORROSION CRACKING OF ZIRCALOY

by Shih-Hsiung Shann
[December 1977]

I. INTRODUCTION

The outstanding high temperature water corrosion resistance and highly desirable nuclear characteristics of zircaloy have made it an excellent cladding material for light water reactors. However, low-ductility failures of the fuel sheath still occasionally occur. The breached cladding can cause the loss of radioactive fission products and fuel-coolant interaction. It points the need for understanding of the fracture mechanism and prevention methods.

The temperature range of fuel cladding eliminates the possibility of liquid metal embrittlement (7), and the fractography of cracked sheath resembles that of stress corrosion cracking in the laboratory (7). These suggest that stress corrosion cracking is the possible mechanism.

Previous works (1-12) proved molecular iodine and stress in 250°C to 500°C can cause low-ductility failure of zircaloy. Most are based on unirradiated specimens. Wood et al. (6,11) tested irradiated samples, but no literature that concerned simultaneous irradiation and stress corrosion have yet been found.

In the present work, radiation, stress and a corrosive agent are applied to the test specimen simultaneously. Iodine can be released from cesium iodine by radiation (14). So cesium iodine is also used (in addition to molecular iodine) as corrosive agent in this experiment. Measurement of stress-rupture properties of zircaloy in the presence of stress corrosion agents and simultaneous irridation is the object of the present experiment.

II. EXPERIMENTAL

Work on stress corrosion cracking of zircaloy-4 was started in April, 1977. Figure 1 shows the design and set up of the apparatus. A 6-inch steel tee is connected to the Van De Graaff accelerator and to a 6" oil diffusion pump. Uniaxial stress is generated in the tensile specimen by weights.* The corrosive agent CsI is supplied by a Knudsen cell heated to 600°C. Molecular iodine can also be used by feeding into the vacuum system through small-diameter tubing (doser). The proton beam from a Van De Graaff accelerator is the radiation source. Both specimen and Knudsen cell are heated electrically. Both I_2 and CsI impinge on a ~¼ inch diameter spot of the specimen as molecular beams. The intensity of these beams is equivalent to a pressure of $\sim 10^{-4}$ torr. Specimen temperature is measured by the IRCON 300 infrared pyrometer. Stress corrosion cracking occurs in the temperature range 250°C to 500°C, and the present system will operate from 300°C to 450°C.

III. RESULTS

Six uniaxial control specimens, with only stress present, but without corrosive agents or radiation, were tested at 350°C. The results are plotted as time-to-failure versus stress in Figure 2. The experimental rupture times are about ten times shorter than those reported in the literature for the same stress in biaxial (tube burst) tests.

There are several possible reasons for very short rupture times, and experimental modification to avoid them.

A) The weight load line is not straight (Figure 3)

Under this condition, a moment is added to the specimen besides the axial load. The original design of the sample mounting is showin in Figure 3a. It can only compensate for a moment in one direction. There are three possible conditions of misalignment shown in Figures 3b, 3c, 3d.

---

* Specimens were fabricated from zircaloy-4 plate graciously supplied by R. Jones of the Stanford Research Institute, Palo Alto.

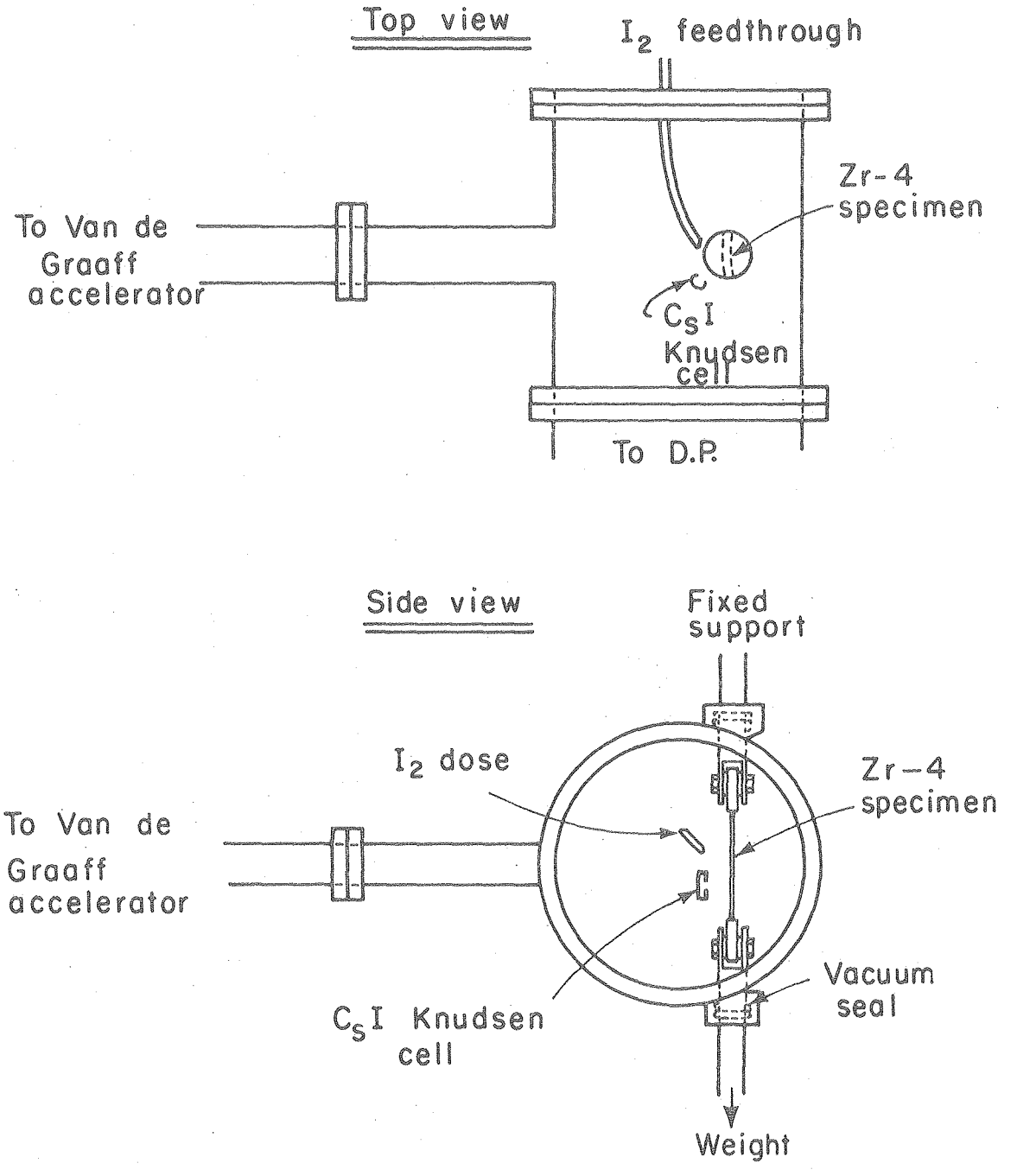

Fig. 1. Experimental arrangement for uni-axial testing.

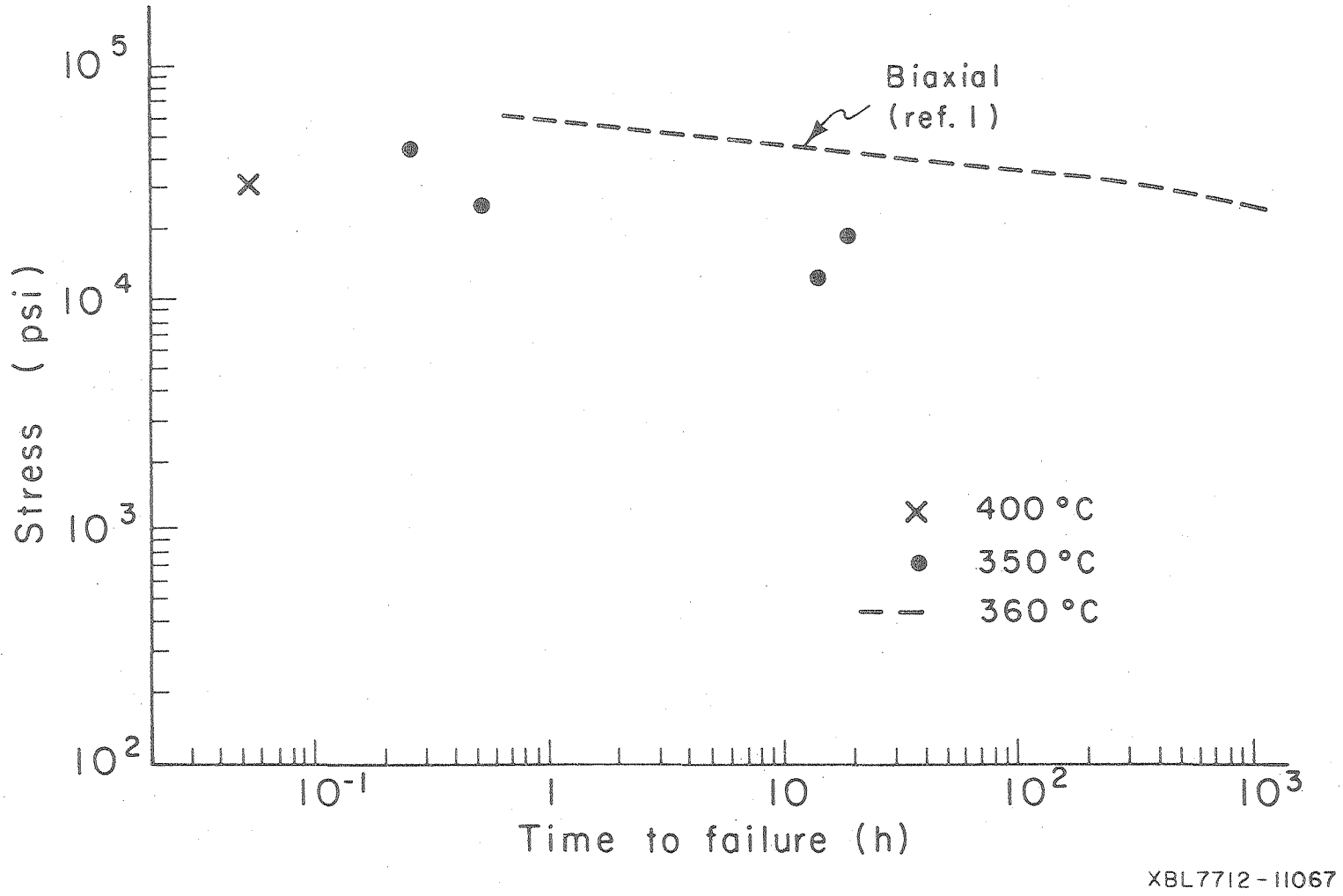

Fig. 2. Stress-rupture curve of control specimens.

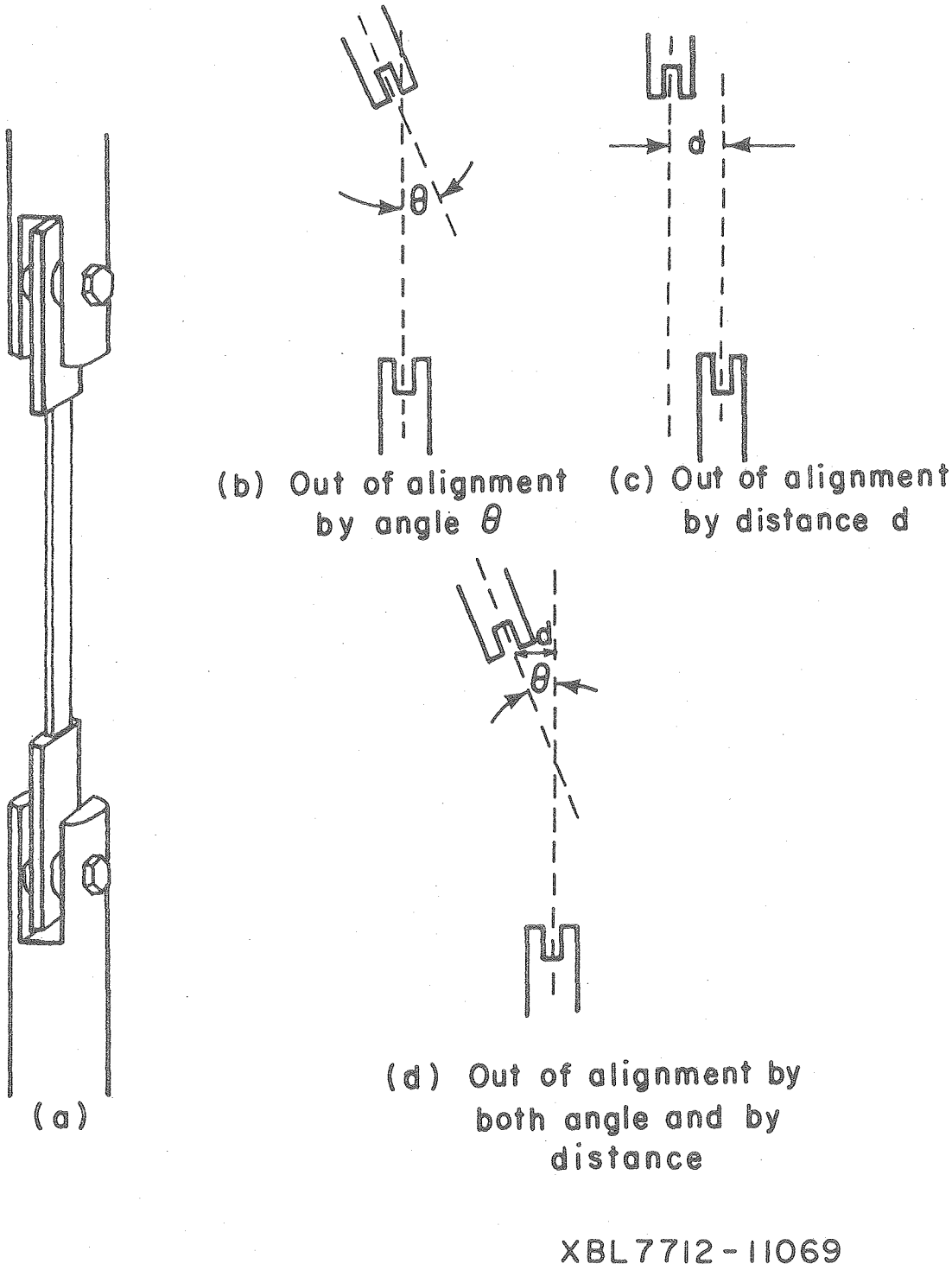

Fig. 3. Original design of specimen mounting device (a) and the conditions of off-vertical loading (b,c,d).

By using universal joints on each end of the specimen (Figure 4), moments in both directions can be eliminated. This modification did not produce longer rupture times, though.

B) Improper control of temperature

Time-to-failure versus stress curve is very sensitive to temperature. The original heating equipment did not have any feedback control. For the 350°C tests, the temperature continuously varied by ±20°C. If time-to-failure is longer than ten hours, the average temperature rose or fell overnight by 70°C to 80°C without manual control. An electronic control system has been installed to compare the output voltage of a thermocouple with a preset standard and to operate a relay in order to turn on or turn off the heating current. The temperature can now be controlled within ±5°C of the set temperature.

C) Uniaxial testing

The previous works concentrated on biaxial testing, but the present experiment is uniaxial. The yielding condition under biaxial loading depends on the ratio of two stresses (15). Coordinate axes x_1, x_2, x_3 are taken parallel to the rolling, transverse, and through-thickness directions, respectively. Uniaxial yield strengths are X_1, X_2, and X_3 respectively. σ_1 and σ_2 are the applied stresses in x_1 and x_2 direction. For special case $X_1 = X_2$ and $X_1 \neq X_3$, the yield condition for biaxial stresses can be expressed as:

$$\sigma_1^2 + \sigma_2^2 - \sigma_1\sigma_2\left[2 - \left(\frac{X_1}{X_3}\right)^2\right] = X_1^2 \qquad (1)$$

Define a material property R by

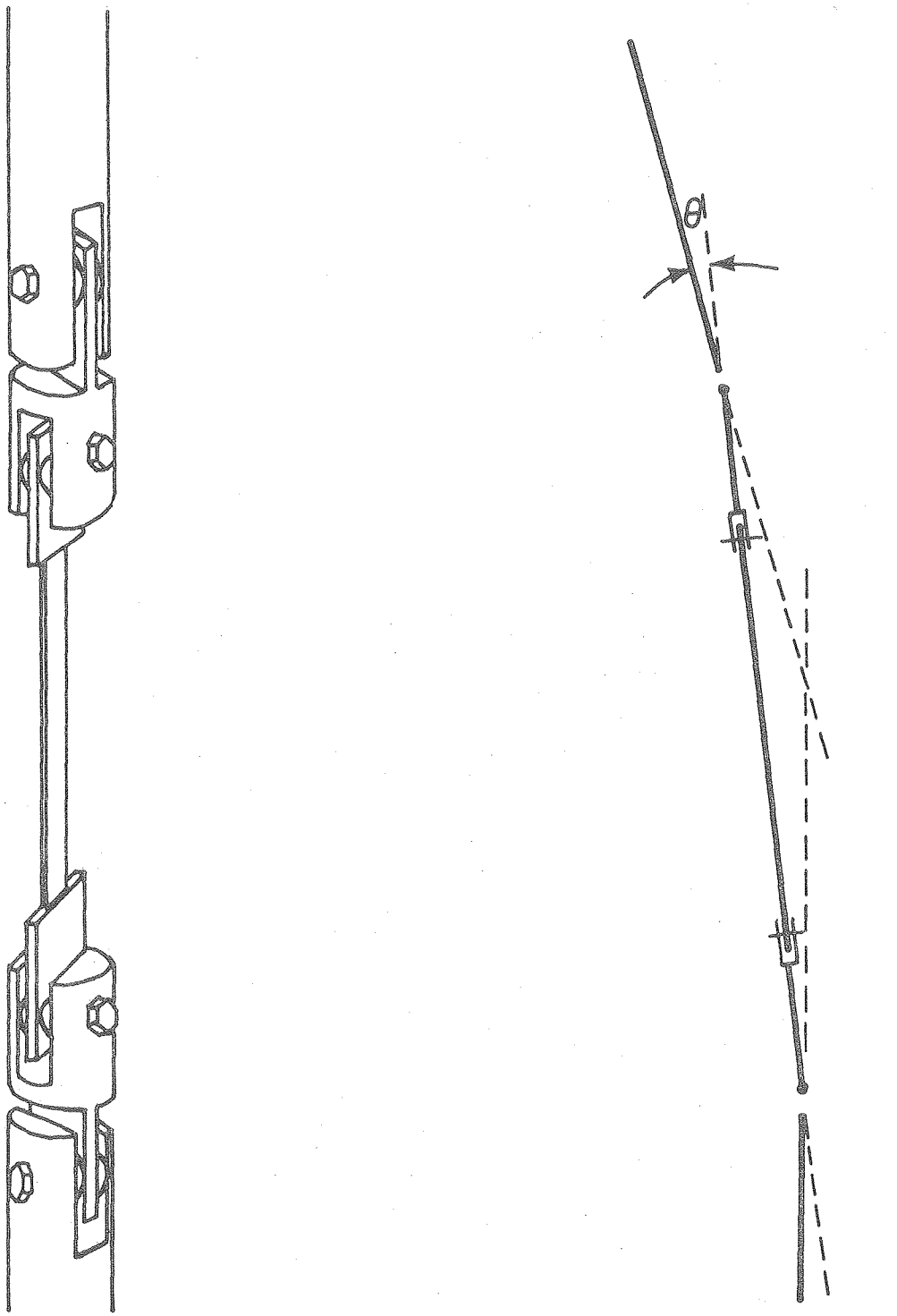

Fig. 4. Improved design of specimen mounting device and the condition of off-vertical loading.

$$X_3 = X_1\sqrt{\frac{1+R}{2}}$$

R is 1.7 for zirconium (15). Taking $\alpha = \sigma_2/\sigma_1$, Eq. (1) can be rewritten as

$$\sigma_1^2 \left[1+\alpha^2-\alpha\left(\frac{2R}{R+1}\right)\right] = X_1^2 \qquad (2)$$

For tube burst experiments,

$$\sigma_z = \sigma_1 \ , \ \sigma_\theta = \sigma_2 \quad .$$

$$\alpha = \sigma_\theta/\sigma_z = 2$$

From Eq.(2)

$$\frac{\sigma_1}{X_1} = 1.934$$

Therefore,

$$\frac{\sigma_\theta}{X_3} = \frac{\sigma_2}{X_3} = \frac{2\times1.934}{1.7} = 2.29$$

If the experimental uniaxial stresses in Figure 2 are multiplied by 2.29 and the time-to-failure replotted versus the new stresses (Fig. 5), the data are comparable to biaxial stress results of previous works (16).

IV PLANNED EXPERIMENTS

There exists a threshold stress which must be exceeded for stress corrosion cracking to occur (1,6,8,12). Viden et al (8) concluded that it is

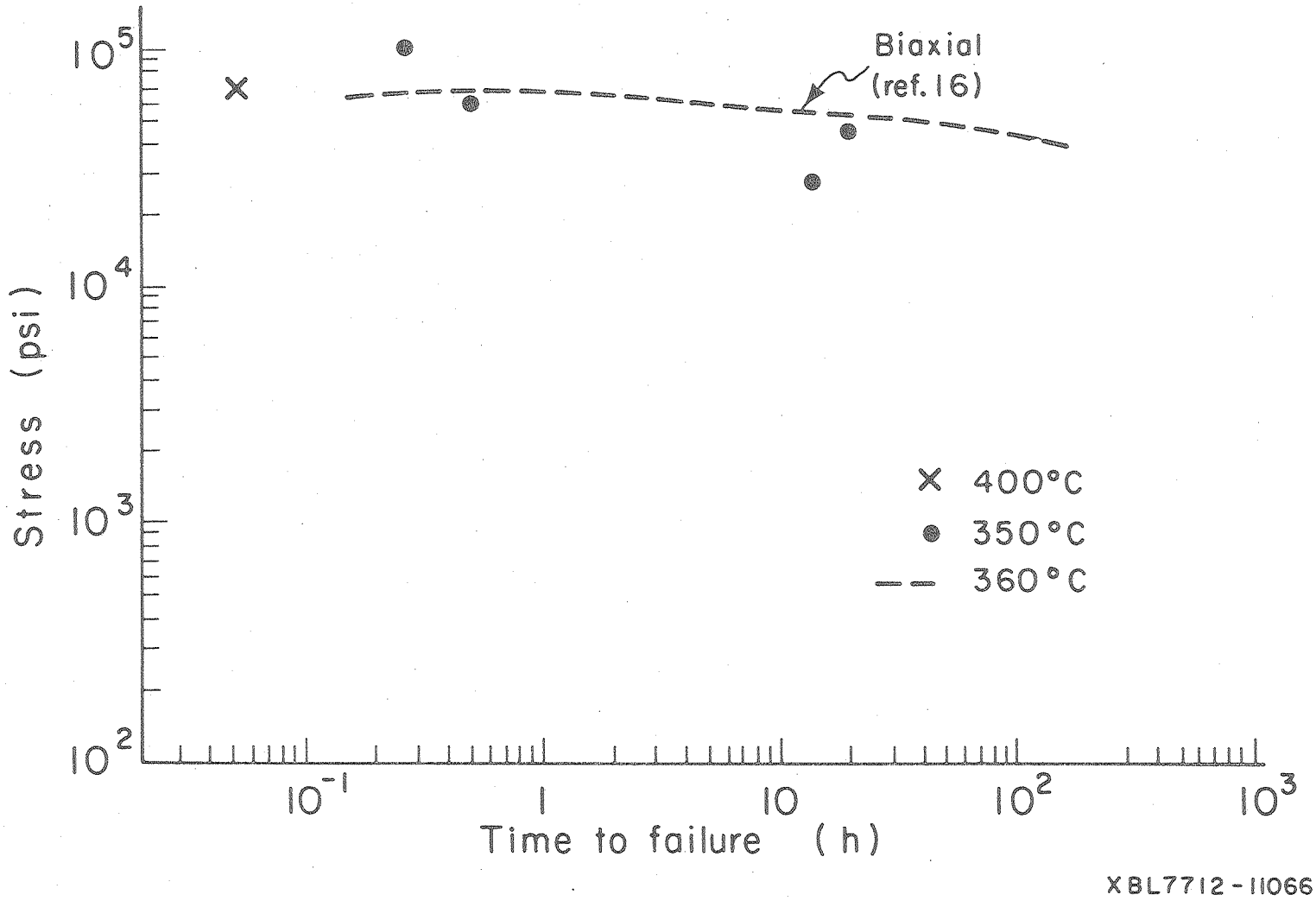

Fig. 5. Control specimen time-to-failure corrected to biaxial loading.

difficult to predict the threshold stress from traditional mechanical properties.

In order to find the difference in time-to-failure between control and corroded/irradiated specimens, a reasonably long (>10 hrs) time-to-failure of control specimens is necessary. From the discussion in section IIIC, it is obvious that yield stress for uniaxial testing is much lower than that of bi-axial testing. It is impossible to get long time-to-failure for stesses higher than threshold stress in a uniaxial test. Garlick et al (2) reported that efforts to initiate stress corrosion cracking in wire samples under uniaxial loading were unsuccessful.

The present experiment was switched to a tube-burst (biaxial) test mode. One-half inch OD tube samples (ground to 10 mil wall thickness) internally pressurized by argon are connected to pressure transducer and a filling valve (Figure 6). The assembly is placed in the vacuum system and heated. To prevent damage to diffusion pumps, a floating mandrel is inserted inside the tube specimen to cut down the gas volume. When the specimen fails, <0.01 moles of gas will flow into the vacuum system. The Van de Graaff accelerator will be protected from the gas burst by a "slammer" valve (17) which has a reaction time of <3 msec after a trigger signal is received from the ion gauge. This time interval is shorter than the travel time of the gas pulse down the accelerator beam tube.

In order to insure that both the proton beam and the I_2 or CsI molecular beams strike the thinnest area of the specimen (where rupture will occur), a thickness scan of the tubing will be done by radiography utilizing Am-241 γ-rays (60 keV).

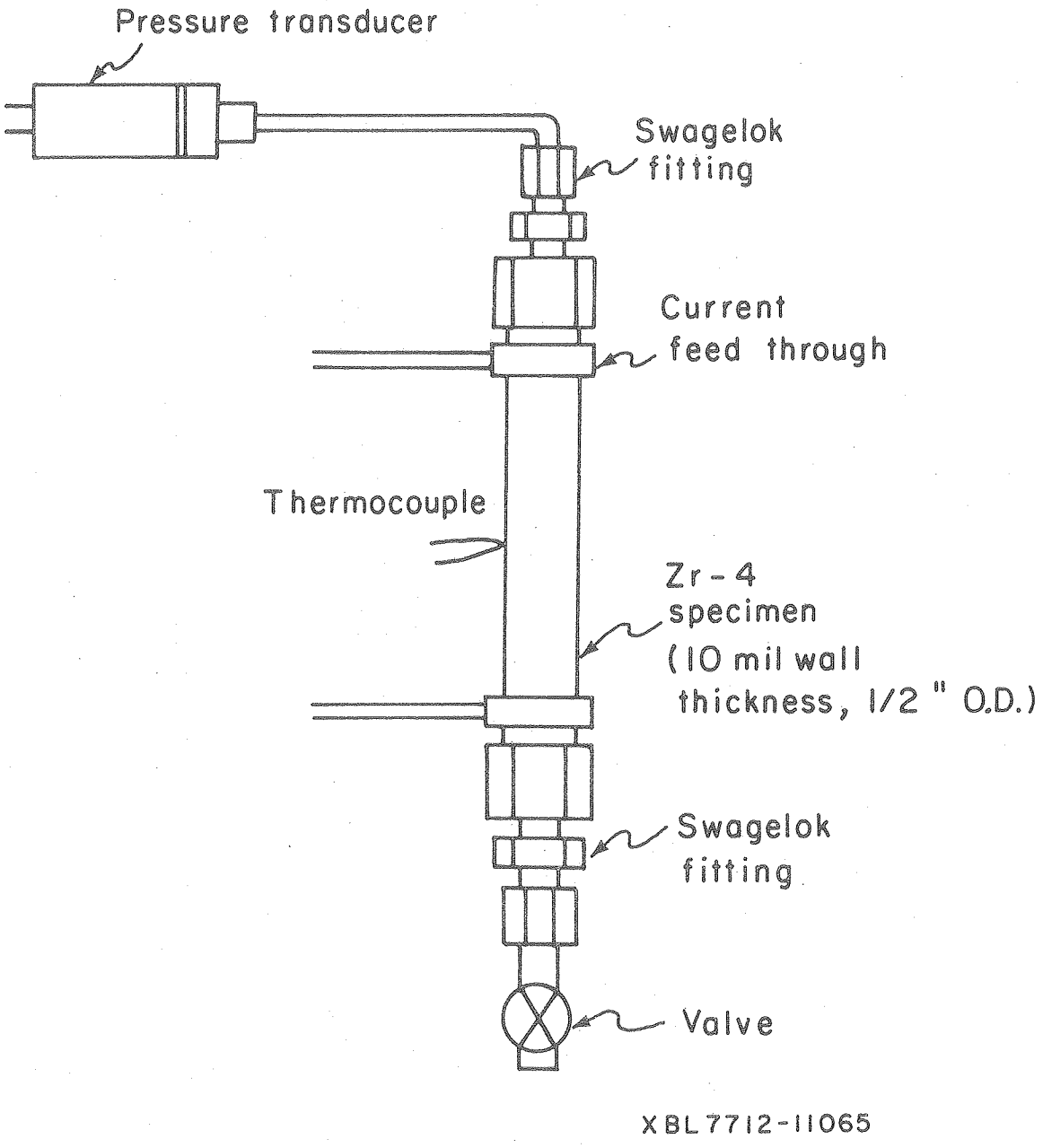

Fig. 6. Specimen assembly for tube burst testing.

REFERENCES

1. C. C. Busby, R. P. Tucker and J. E. McCauley, J. Nucl. Mater., 55, (1975) 64-82.

2. A. Garlick and P. D. Wolfenden, J. Nucl. Mater., 41, (1971) 274-292.

3. P. H. Kreyns, G. L. Spahr and J. E. McCanley, WAPD-TM-1203(1976).

4. J. G. Weinberg, WAPD-TM-1048 (1974).

5. R. P. Tucker, P. H. Kreyns and J. J. Kearns, WAPD-TM-1248 (1976).

6. J. C. Wood, J. Nucl. Mater., 45, (1972/73) 105-122.

7. J. C. Wood, B. A. Surette, I. M. London and J. Baird, J. Nucl. Mater., 57, (1975) 155-179.

8. K. Videm and L. Lunde, Annals of Nuclear Energy, 3, (1976) 305-313.

9. I. Aitchison and B. Cox, Corrosion, 28, (1972) 83-87.

10. B. Cox, Corrosion, 28, (1972) 207-217.

11. J. C. Wood, Nucl. Technology, 23, (1974) 63-79.

12. A. Garlick, J. Nucl. Mater., 49 (1973/74) 209-224.

13. K. Elayaperumal, P. K. De and J. Balachandra, J. Nucl. Mater., 45, (1972/73) 323-330.

14. D. Cubicciotti and J. H. Davis, Nuclear Science & Engineering, 60, (1976) 314-319.

15. W. A. Backofon, W. F. Hosford, Jr. and J. J. Burke, Trans. ASM, (1962) 264-267.

16. R. Jones (Stanford Research Institute) Personal Communication (1977).

17. R. A. Gough, R. Lam, C. Martinez and D. Morris, Nuclear Instruments and Methods, 138 (1976) 415-419.

THE SURFACE CHEMISTRY OF EPITAXIAL SILICON DEPOSITION BY THERMAL CRACKING OF SILANE

by M. Farnaam

I. INTRODUCTION

Production of epitaxial layers of silicon on a substrate by the cracking reaction $SiH_4(g) \rightarrow Si + 2H_2(g)$ is a widely used and intensively studied process. This technique is utilized extensively in the semiconductor industry and more recently in the fabrication of photovoltaic devices for direct solar energy conversion to electricity. Until very recently, atmospheric pressure reaction was the standard method for the chemical vapor deposition (CVD) growth process. Recently, low pressure chemical vapor deposition (LPCVD) reaction ($\sim$ 0.5 torr, 640 °C) was found to give lower costs, higher productivity, and better uniformity compared to the atmospheric pressure method (1).

The overall deposition process can be divided into two subprocesses: (1) the surface decomposition of the silicon-bearing gas to produce silicon adatoms and, (2) the incorporation of the silicon adatoms into an epitaxial layer. The second aspect has received the most attention in the literature; the growth process is driven by the supersaturation of the surface with silicon adatoms but does not depend upon their source (i.e., whether produced from a CVD process or by condensation of silicon vapor). The first subprocess contains all the surface chemistry of the overall process, and is the object of the present experiment.

The meager literature on the surface chemistry of the silane cracking reaction (2,3,4) is based upon conventional techniques of heterogeneous kinetics (i.e., steady state measurements of the rate of H_2 production) and results in contradictory mechanistic interpretations. Our experiment utilizes a modulated molecular beam method, thereby permitting more detailed probing of the surface processes by use of phase lag measurements

than can be achieved by steady state kinetic studies (5).

II. EXPERIMENTAL

A. Molecular Beam Apparatus

The apparatus shown in Fig. 1 is composed of three vacuum chambers:

a) The *source chamber* (diffusion pumped), in which a modulated beam of silane is generated.

b) the *target chamber* (diffusion pumped) in which interactions between the silane and the silicon substrate take place. This chamber also contains an ion gun for sputter-cleaning the specimen.

c) the *detection chamber* (ion pumped) containing a quadrupole mass spectrometer for detecting species emitted from the surface.

The silane molecular beam, generated in the source tube, is chopped by a rotating slotted wheel to form a modulated beam, then passes through the 0.8 mm diameter hole to bombard the substrate at a 45° angle. The scattered reactant and product (H_2) pass through a 1.6 mm diameter hole to reach the detection chamber to be detected by the mass spectrometer.

B. Specimen Preparation

The crystals were purchased from Materials Research Corporation in the form of 1 inch diameter disks with (111) surfaces as faces. Specimens with a cross section of 6 mm x 2.5 mm were cut from the disks and the (111) faces were polished. The samples were cleaned in acetone, methanol, methyl ethyl ketone, and ethanol. They were subsequently dipped in an acid etch solution of 6 parts HNO_3 (70%), 3 parts HF (48%) and 2 parts acetic acid for about 40 seconds, then rinsed in distilled water.

C. Heating and Temperature Measurement Methods

The specimens are held in the vacuum system by tantalum clips and heated resistively. The temperature of the reaction surface is measured by an optical pyrometer.

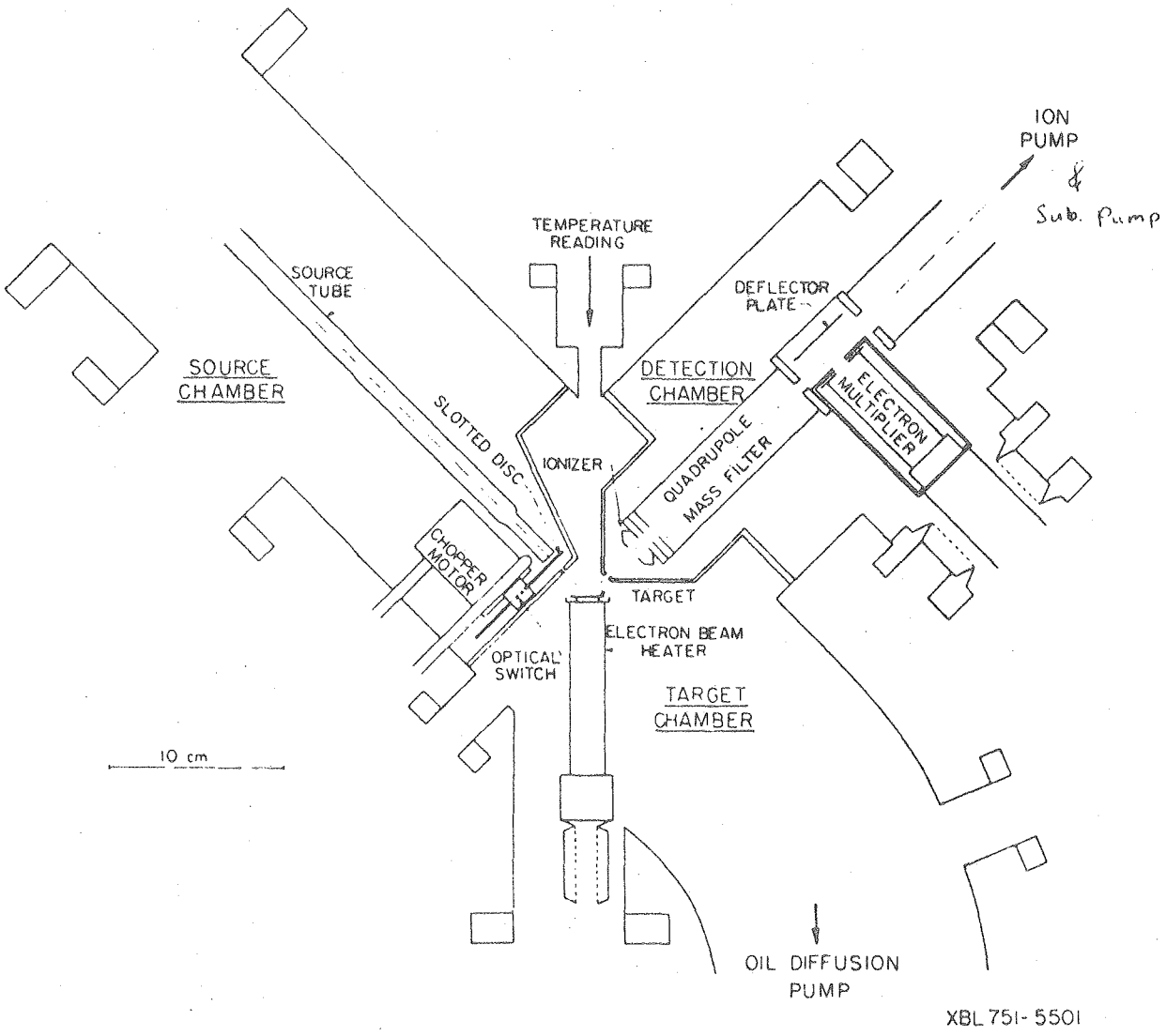

Fig. 1. Apparatus cross-section.

III. RESULTS

Below ∿ 1000 K, a temperature-independent H_2^+ signal about 2% of the intensity of the SiH_3^+ signal from reflected silane is present because of fragmentation of the silane in the mass spectrometer ionizer. At higher temperatures the apparent reaction probability (i.e., the ratio of the H_2^+ signal amplitude to that of SiH_3^+) increased with temperature, which indicated the onset of detectable silane cracking on the substrate. The H_2^+ signal also exhibited a phase lag with respect to the SiH_3^+ signal. The true reaction product signal was determined by subtracting (vectorially) the H_2^+ signal due to silane fragmentation in the mass spectrometer from the total H_2^+ signal.

H_2 reaction probabilities and phase lags were measured as functions of silane beam intensity (10^{-5} to 10^{-4} torr equivalent pressure), substrate temperature (1000 - 1500 K) and modulation frequency (10 to 1000 Hz). After this series of experiments, the specimen was examined by scanning electron microscope. Instead of a smooth growth surface, islands were formed (Fig. 2). Because these islands may falsify the surface chemical kinetics (2 - 4), the molecular beam data were not fitted to a detailed reaction mechanism, which will be done only when smooth surfaces result from the experiment.

Additional experimentation showed that islands formed simply upon heating to ∿ 1400 K in the absence of the silane beam. Moreover, islands could not be avoided by sputter cleaning the surface by in situ ion bombardment, either prior to heating or at elevated temperatures. Ion cleaning merely had the effect of subdividing the island, making more but smaller ones.

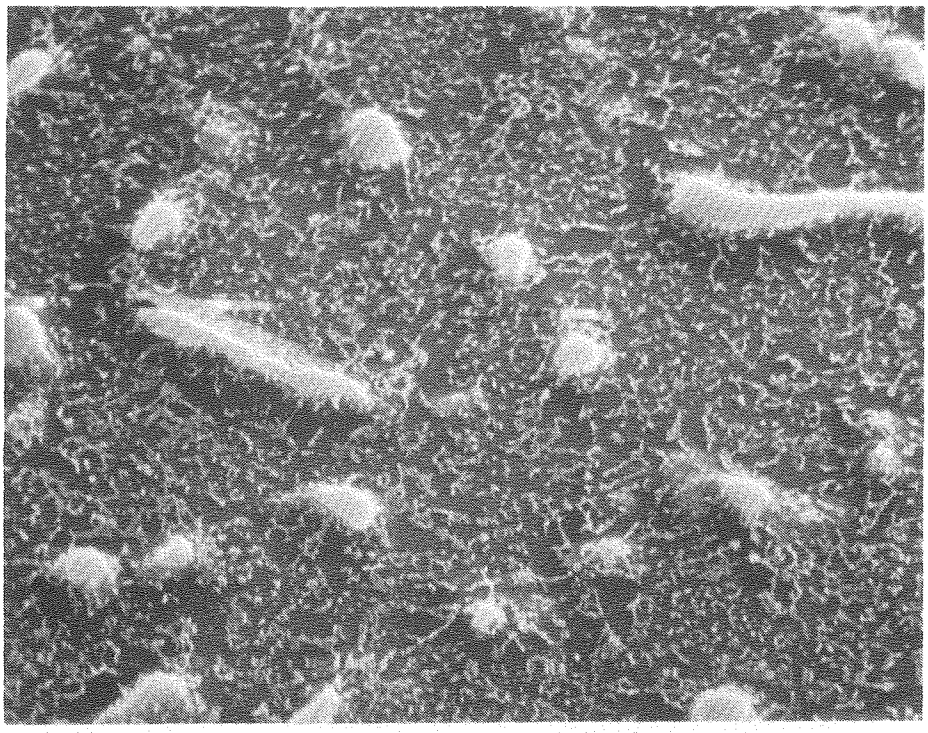

surface after heating

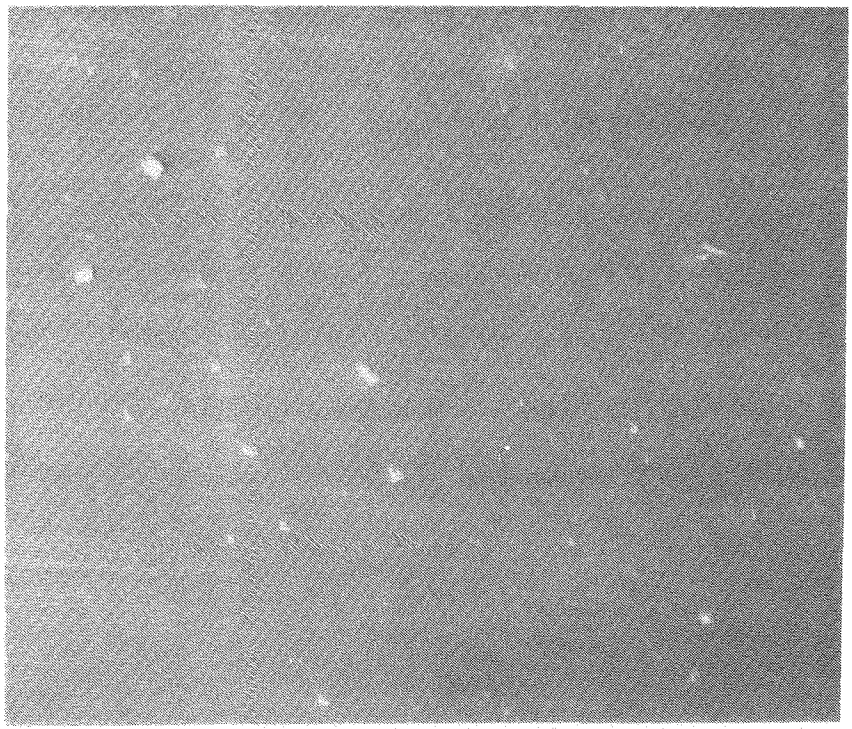

original surface

XBB 7712-12551A

Fig. 2. Island growth on single crystal of silicon due to heating in a vacuum of 10^{-8} torr. Top photo shows surface after heating, bottom photo shows the original surface.

IV. PLANNED EXPERIMENTAL MODIFICATIONS AND CHEMICAL KINETIC STUDIES

To avoid island growth, in subsequent experiments, three approaches are being followed.

First, crystals are being purchased from Dow Corning Corp. These are of higher purity (0.2 ppm O and 0.2 ppm C, resistivity of 1000 Ω-cm) than those available from MRC (20 ppm O, 1 ppm C, resistivity 100 Ω-cm).

Second, the 13-step cleaning procedure suggested in Ref. 6 will be used.

Third, if the first two changes do not eliminate island growth, the diffusion pump on the target chamber will be replaced by an ion pump to permit attaining a base pressure of $\sim 10^{-10}$ torr (it is currently $\sim 10^{-8}$ torr).

Once the island growth problem is eliminated, the kinetic studies of the silane cracking reaction will be continued along the following lines:

a) Repeat the standard molecular beam experiments to see whether the kinetics are affected by the presence (or absence) or islands.

b) Conduct isotope exchange experiments, utilizing a modulated SiH_4 beam simultaneously impinging on the target with a steady SiD_4 beam from a smaller doser installed directly in the target chamber. The purpose of this experiment is to attempt to detect the mixed reaction product HD, which would indicate that atomic hydrogen is a reaction intermediate on the silicon surface.

c) Conduct experiments on Si (100) surfaces in addition to the Si (111) surfaces which are now being investigated. Incorporation of surface-adsorbed mobile silicon atoms into the crystal lattice is throught to be much easier in the (100) surface than on the (111) surface. This experiment will seek to determine if the degree of supersaturation of the surface with adsorbed silicon atoms affects the kinetics of the silane cracking reaction which precedes surface deposition and growth.

References

1. R.S. Rosler, Solid State Tech., p 63, April (1977)

2. B.A. Joyce et. al., Phil. Mag., 14, 289, 301 (1966) and 15, 1167 (1967).

3. R.C. Henderson et. al., Surf. Sci., 30, 310 (1972).

4. R.F.C. Farrow, J. Electrochem. Soc., 121, 899 (1974).

5. R.H. Jones, D.R. Olander, W.J. Siekhaus, and J.A. Schwarz, J. Vac. Sci. Technol. 9, 1429 (1972).

6. S.P. Murarka et. al., J. Appl. Phys. 48, No. 9, (1977).

THERMAL GRADIENT MIGRATION OF METALLIC INCLUSIONS IN UO_2

by R. L. Yang

I. Introduction

As a result of the steep temperature gradient in FBR fuel the fission products move away from the location where they are produced. The noble metals Ru, Tc, Rh and Pd precipitate into a distinct metallic phase in the fuel. It was observed that these inclusions move bodily up the temperature gradient in the reactor fuel. Occasionally big chunks of metallic fission product are found in the central void.

Although there are many analyses of irradiated fuel (1,2) current knowledge on the behavior of metallic fission product is largely incomplete. This is due to the fact that the behavior of fission products in the fuel is complicated and depends on many interlinked parameters (e.g. temperature, O/M ratio, and the presence of other fission products, etc.) that are difficult to evaluate.

Recent studies on the migration of metallic fission-product inclusions have been done by Michels and Poeppel (1) and Schumacher et. al. (3)

Michels and Poeppel measured the migration velocity of solid fission-product inclusions in uranium - plutonium mixed oxide under irradiation. They found that inclusions move in the direction of increasing temperature, and the measured velocity is in agreement with the calculated velocity based on a surface diffusion mechanism. However, their data are quite scattered. This is probably due to the difficulties inherent in post-irradiation analyses described above. Schumacher et. al. (3) measured the migration velocity of inclusions in an out-of-pile experiment. Small fission product inclusions (all less than 0.3 μm) were added uniformly to the mixed oxide by a coprecipitation technique. Heat treatment of these materials in a simulated reactor thermal gradient caused

the metallic inclusions to migrate. During migration, coagulation took place. After heat treatment, specimens were cut and polished. The size distribution of inclusions larger than 0.3μ were measured and migration rate was calculated. In this experiment, small inclusions (< 5μ) move according to surface diffusion mechanism. Larger inclusions (> 5μ) are practically immobile.

The purpose of the present experiment is to build a temperature gradient furnace and to study the migration mechanism of metallic inclusions in a controlled condition in the laboratory.

II. Experiment

A temperature gradient furnace which is capable of producing a temperature gradient of 1500 °K/cm at a maximum temperature of 3000 °K was constructed for use in vacuum (Fig. 1)

In this set-up, the UO_2 specimen is contained in a tungsten crucible which is closed at the top to avoid loss by vaporization. The top of the crucible is heated by electron bombardment and the bottom temperature is controlled by a molybdenum rod acting as a heat sink. The upper temperature is measured by an automatic optical pyrometer and the bottom temperature by a W/W-Re thermocouple. The UO_2 specimens consist of a thin wafer (1 mm thick) and a pellet of the same diameter and 1.2 cm thick. A layer of 3-6 micron spherical tungsten powder is inserted between the UO_2 wafer and the UO_2 pellet to simulate the metallic fission product inclusions. The wafer thickness is chosen so that it is thin enough that the temperature in the wafer is high enough for the inclusions to move at a reasonably high rate, yet thick enough for the inclusions to migrate a measureable distance. The tungsten powders are first suspended in methyl alcohol and then further dispersed in a ultrosonic cleaner for about 5 minutes. After turning the ultrasonic cleaner off, a UO_2 pellet is placed into the liquid for $\sim$ 20 seconds

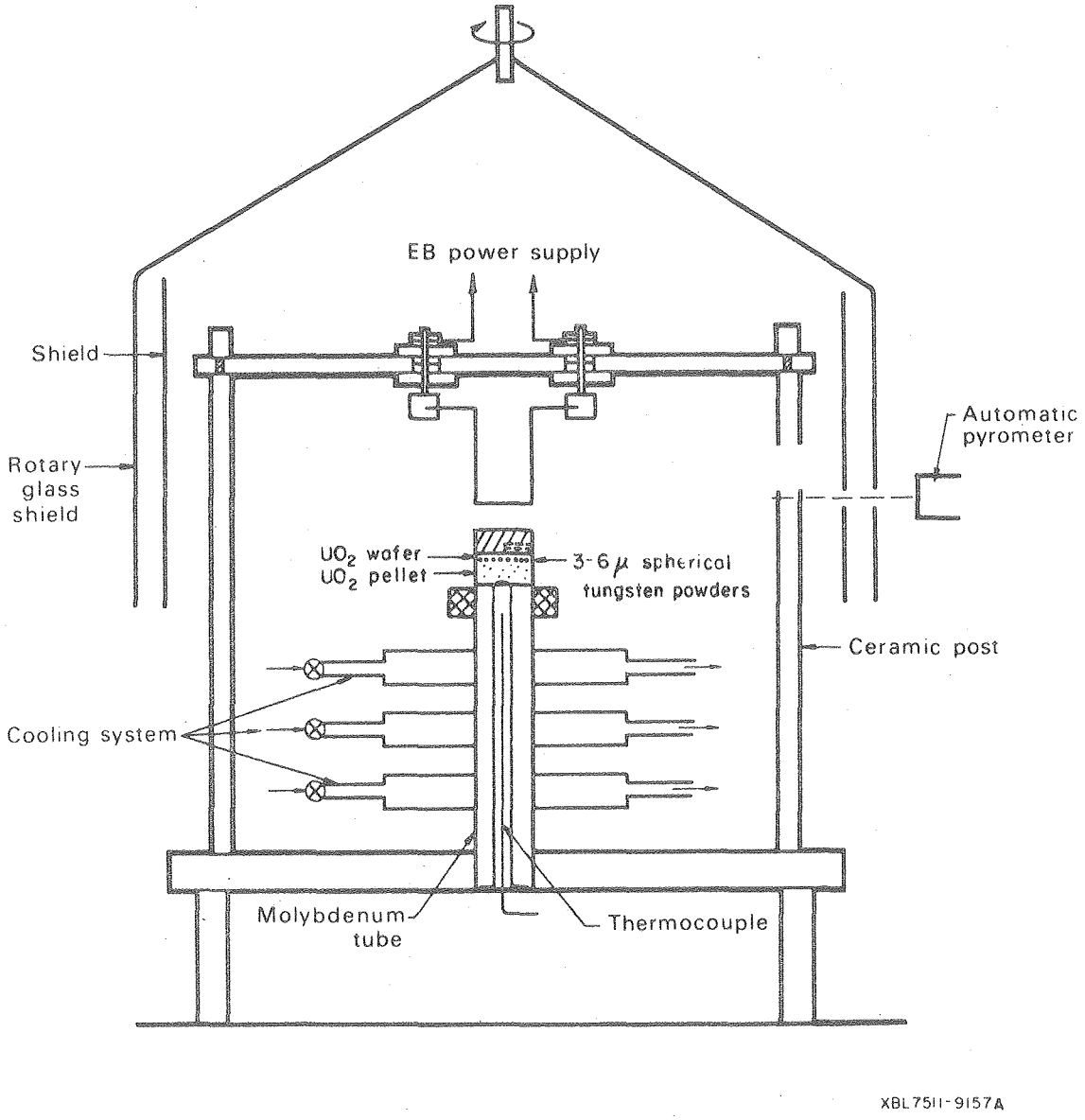

Fig. 1. Temperature gradient furnace.

to collect a thin layer of tungsten spheres. The specimen is then assembled as described above. Following thermal gradient heat treatment, the pellets are sectioned and observed microscopically.

III. Theory

The possible mechanisms for the migration of inclusions under the temperature gradient are surface diffusion and volume diffusion. The migration velocity (V_s) calculated from the surface diffusion mechanism gives (4,5):

$$V_s = \frac{2 D_s \Omega^{1/3} Q_s^*}{kT^2} \left(\frac{3k_s}{2k_s + k_i}\right) \frac{1}{R} \left(\frac{dT}{dz}\right) \qquad (1)$$

where D_s = surface diffusinity of UO_2 (actually, the interfacial diffusion coefficient of UO_2 between UO_2 and tungsten)

k_s = thermal conductivity of UO_2

k_i = thermal conductivity of inclusion

Ω = atomic volume of UO_2

Q_s^* = heat of transport of UO_2 for surface diffusion

R = radius of inclusion

k = Boltzmann constant

T = absolute temperature

$\frac{dT}{dz}$ = temperature gradient far away from inclusions

The velocity calculated from volume diffusion mechanism (V_v) is (4,5):

$$V_v = \frac{D_v Q_v^*}{kT^2} \frac{2(k_s - k_i)}{2 k_s + k_i} \left(\frac{dT}{dz}\right) \qquad (2)$$

where D_v = volume diffusion coefficient of UO_2

Q_v^* = heat of transport for volume diffusion

Note that the surface diffusion mechanism predicts an inverse dependence of migration velocity with particle radius while the velocity according to volume diffusion mechanism is particle-size independent. In addition, since $k_s < k_i$, the inclusions should move up the temperature gradient for the surface diffusion mechanism (with $Q_s^* > 0$) but down the temperature gradient if the volume diffusion process (with $Q_v^* > 0$) is dominant.

The measurement of migration rate of the metallic inclusions as a function of the inclusion sizes should provide a method of establishing the migration mechanism.

As can be seen in equations (1) and (2), the temperature distribution in the sample plays an important role in the migration volocity of inclusions. The temperature distriubtion in the UO_2 specimen has been calculated both analytically and numerically. Fig. 2 shows the temperature distribution in the empty tungsten crucible with heating on the top and radiation heat loss from the sides. The temperature distribution in the empty crucible was used as a boundary condition in solving the heat conduction equation for the uranium oxide sample inside. The results are shown in Fig. 3.

IV. Results

1. After thermal gradient heat treatment ($T(hot) \simeq 2700°K$, $T(cold) \simeq 1400°K$) the sample was sectioned longitudinally, polished and observed microscopically. The samples exhibited remarkable restructuring. Several process, such as sintering, grain growth and pore migration occured. In Fig. 4, the white spherical dots are the tungsten powders, the gray area is uranium oxide. The line of particles indicates the interface between UO_2 wafer and pellet where tungsten powders were inserted before theat treatment. These experiments showed that the gap between the UO_2 wafer and the pellet is completely closed by sintering during the heat treatment.

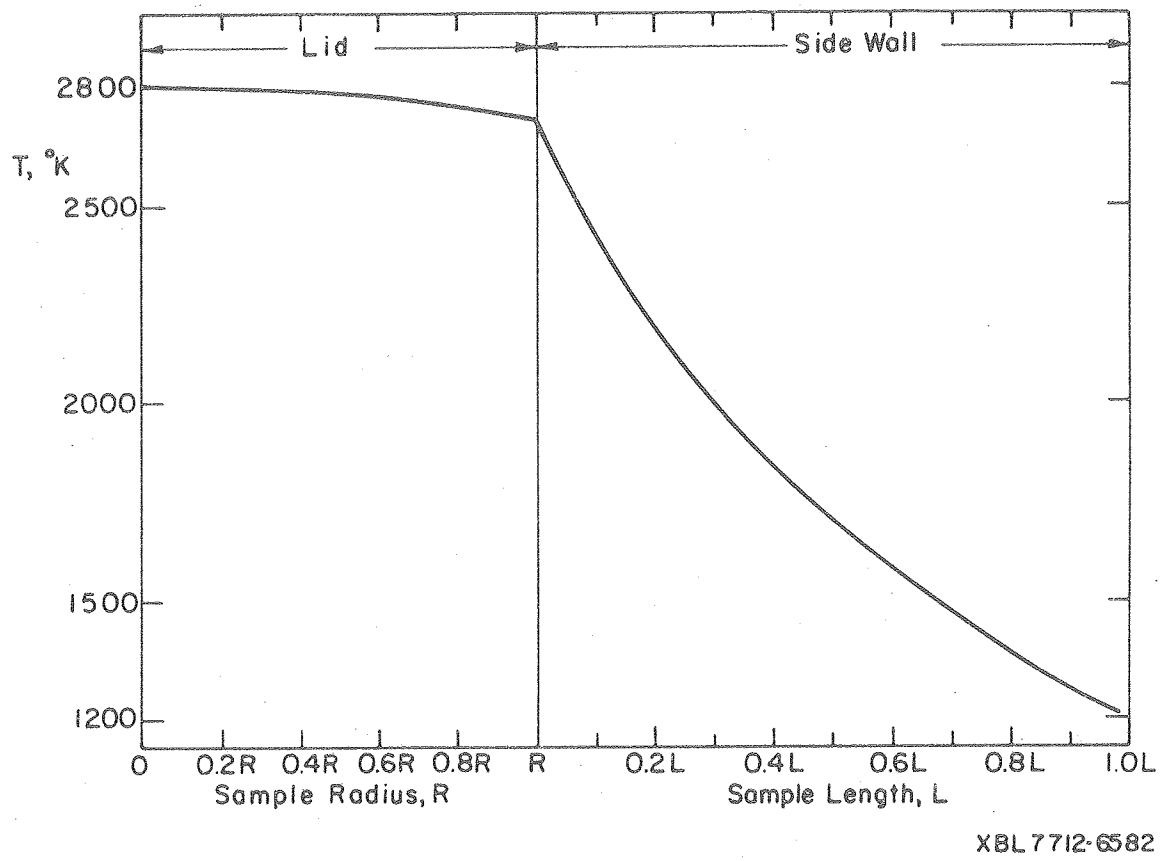

Fig. 2. Temperature distribution in empty tungsten crucible with radiation loss from surface.

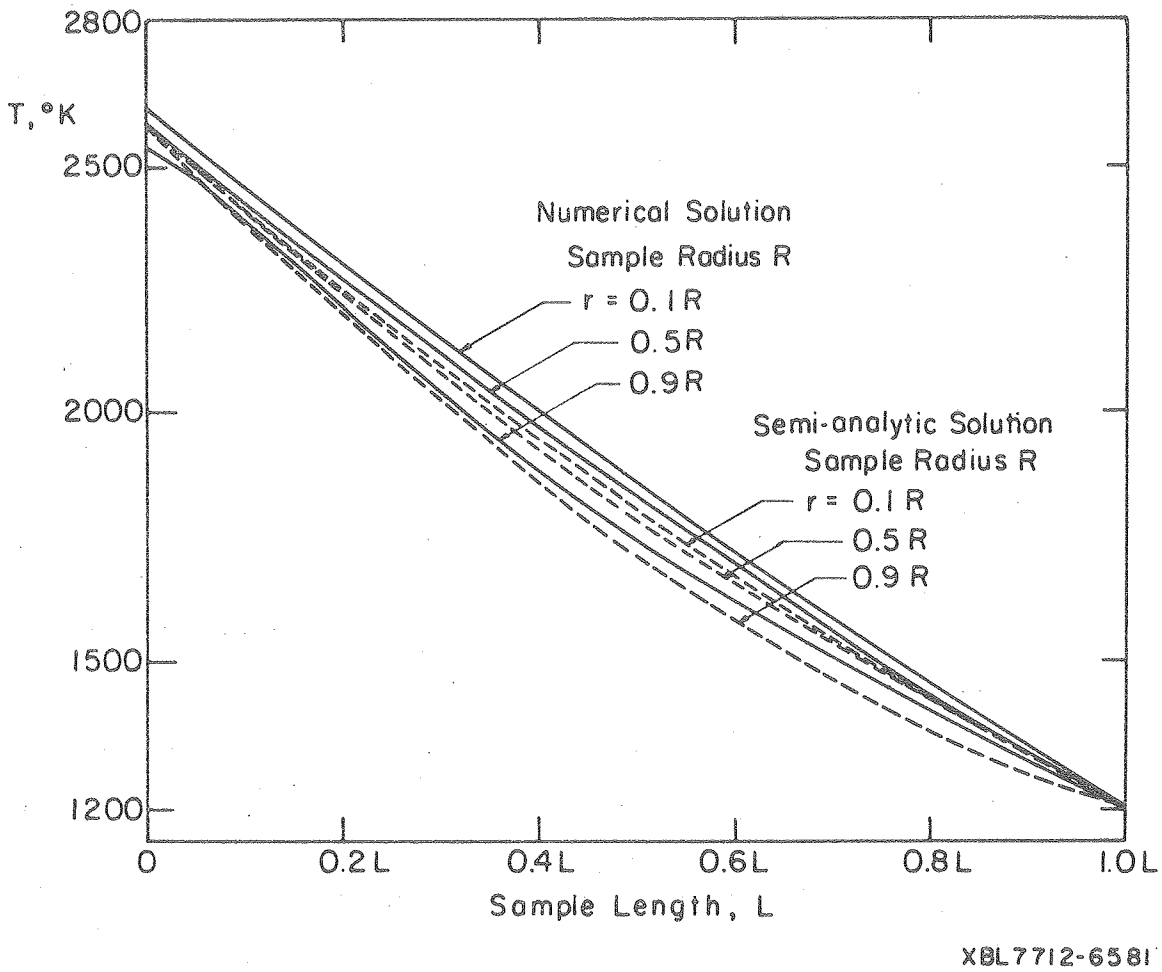

Fig. 3. Temperature distribution in UO_2 sample.

2. We found that the UO_2 reacted with the tungsten powders and the tungsten crucible. We solved this problem by reduced UO_2 in H_2 atmosphere for 4 hours at 1800°C so that the oxygen potential of uranium oxide is low enough not to react with tungsten.

3. After the UO_2 was reduced, we found that UO_{2-x} and tungsten form a low melting eutectic (6,7,8). The top sections of our samples have melted at temperatures as low as 2600 K. This may be due to the impurities in UO_2 which migrate to the hot tungstein-UO_2 interface under temperature gradient. Examining the top of the UO_2 sample with EDAX (Fig. 5), we found precipitates of copper-rich tungstein and nearly pure iron. An analysis by the General Electric Company showed Si, Fe and Cu impurities in the UO_2 we used. To eliminate this problem, we plan to coat the top of UO_2 sample with vacuum-vapor deposited rhenium.

4. Because UO_2 is held at high temperature in vacuum it must be encapsulated to prevent excessive vaporization loss. We have tried CVD (Chemical Vapor Deposition) tungstein crucibles for this purpose. Although the crucible prevented excessive vaporization, we could not achieve the close pellet-to-crucible fit needed to maintain geometric integrity of the UO_2, which is quite plastic at this high temperature. We believe that the direct CVD coating of UO_2 pellets with tungstein would solve the problem. Since we do not have the facilities to do this job, UO_2 specimens were sent to Los Alamost National Laboratory to be coated. They had difficulties depositing tungsten on UO_2 due to the fact the WR_6 and HF attack the UO_2 surface. Their approach to the problem is to sputter a thin film of tungstein on UO_2, then deposit thicker (10 mil) layer of tungsten by CVD.

5. Since the UO_2 samples are about 90% T.C., all the pores migrated toward the hot end during the thermal gradient heat treatment. This leaves a ~2 mm gap between the top of UO_2 and tungsten crucible. In our system,

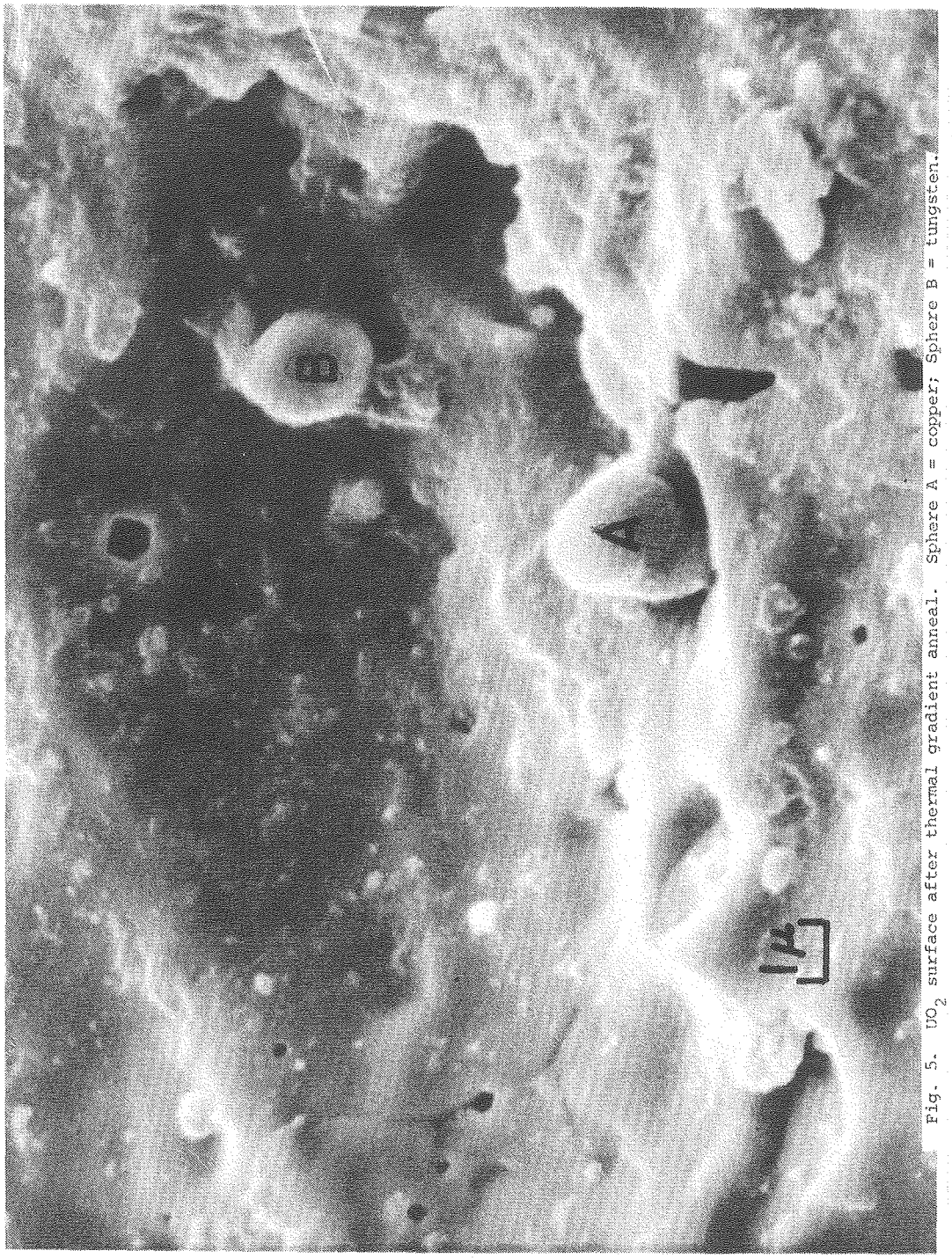

Fig. 5. UO_2 surface after thermal gradient anneal. Sphere A = copper; Sphere B = tungsten.

the center part is hotter than the sides, hence the top surface of UO_2 becomes concave due to vapor transport of UO_2 from the center to the sides through the gas space. Approaches to this problem include: First, to sinter the UO_2 pellet-wafer combination (with the tungstein powder in between) at about 1900°C in H_2. Figure 6 shows that the UO_2 pellet-wafer combination is held together by a molybdenum yoke. The tantalum nut is tightened by a torque wrench to 80 mm-kg. Since the thermal expansion coefficient of molybdenum is smaller than that of UO_2, the UO_2 pellet should be in compression at high temperature. In this way we hope to reduce the porosity in UO_2 and eliminate the gap between the UO_2 wafer and pellet before the thermal gradient migration experiment. Secondly, the electron bombardment filament will be redesigned so that the temperature across the top of the tungsten lid is more uniform, thus reducing the vapor transport through the gap.

References

1. L.C. Michels and R.B. Poeppel, J. Appl. Phys., 44, 3, (1973).

2. R.R. O'Boyle, F.L. Brown and A.E. Dwight, J. Nucl. Mater., 35, 257 (1970).

3. F. D'Annucci, C. Sari and G. Schumacher, Nucl. Technol., 35, 80 (1977).

4. P.G. Shewmon, Trans. AIME, 230, 1134 (1964).

5. F.A. Nichols, J. Nucl. Mater. 30, 143 (1969).

6. R.J. Gerdes, A.T. Chapman and G.W. Clark, Science 167, 979 (1970).

7. A.T. Chapman, G.W. Clark and D.E. Hendrix, J. American Ceramic Soc. 53, 60 (1970).

8. J. Briggs and P.E. Hart, J. Am. Ceram. Soc. 59, 530 (1976).

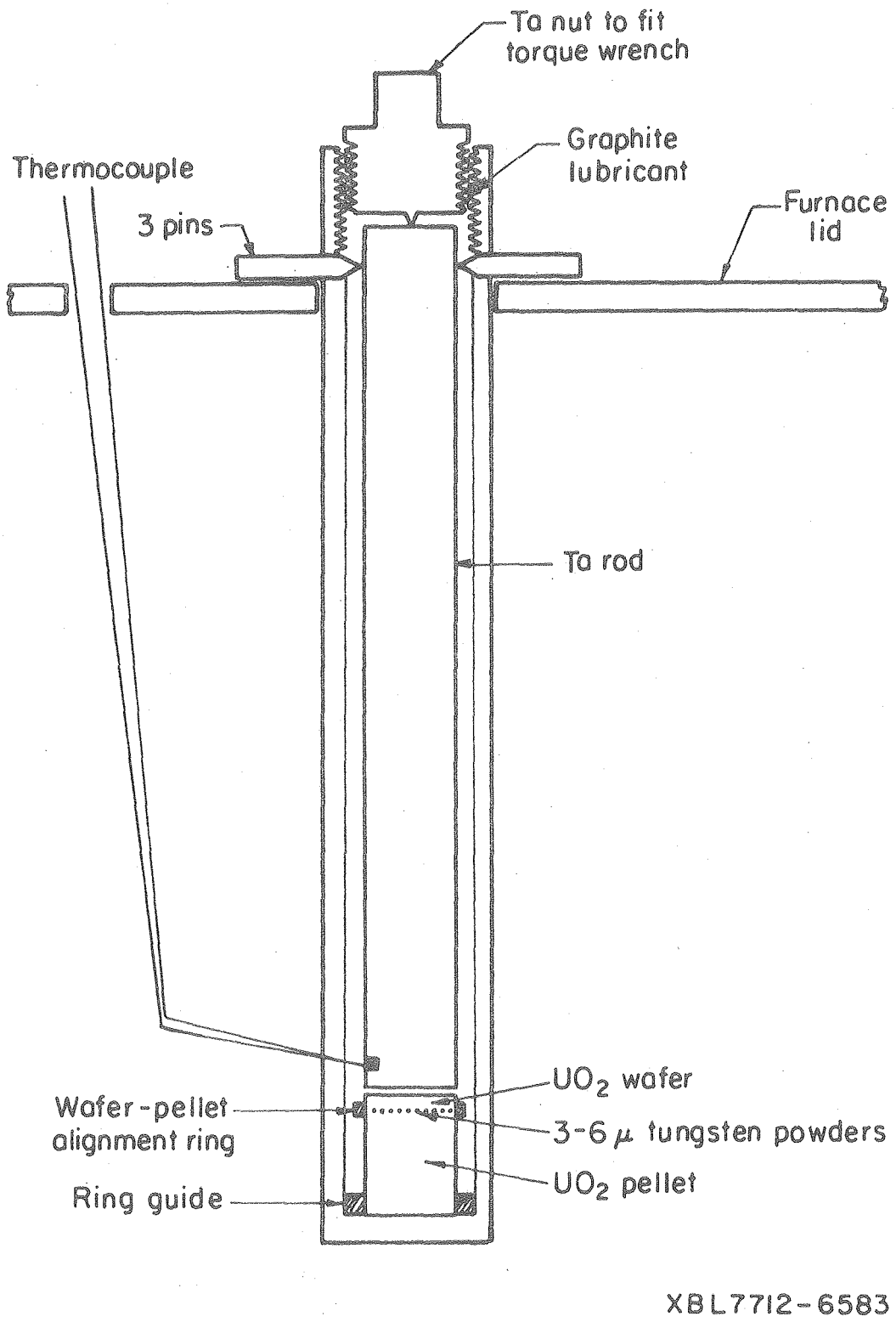

Fig. 6. Molybdenum yoke used in sintering of UO_2.

MOLECULAR BEAM STUDIES OF ATOMIC HYDROGEN REDUCTION OF OXIDES

by Douglas Dooley

I. Introduction

Oxide insulator materials exposed to the hot hydrogen fuel of a CTR plasma will be subject to chemical as well as physical corrosion (1,2). To better understand the nature of the chemical attack, the reduction reactions of thermal atomic hydrogen with various oxides, i.e. UO_2, Al_2O_3, and Y_2O_3, are being studied by the modulated molecular beam method.

Although previous studies have made qualitative observations of atomic hydrogen/oxide reactions and others have predicted corrosion rates based on thermodynamic equilibrium models, there is little information about the elementary reaction steps which comprise the overall reduction reaction and the values of the associated rate constants. This information can be obtained by modulated molecular beam mass spectrometry, which is a technique of studying heterogeneous chemical reactions in a detail not attainable by conventional chemical kinetic experiments (3,4).

II. Experimental

The molecular beam study of the reduction of UO_2 by atomic hydrogen is being conducted in the vacuum apparatus shown in Fig. 1. The reactant atomic hydrogen beam is formed by effusion from a thermal dissociation source and modulated by a mechanical chopper before striking the surface of the heated UO_2 target. H_2O molecules produced by the reduction reaction are detected by a mass spectrometer. The output signal is processed by a lock-in amplifier and analyzed to determine the mechanism of the reduction reaction.

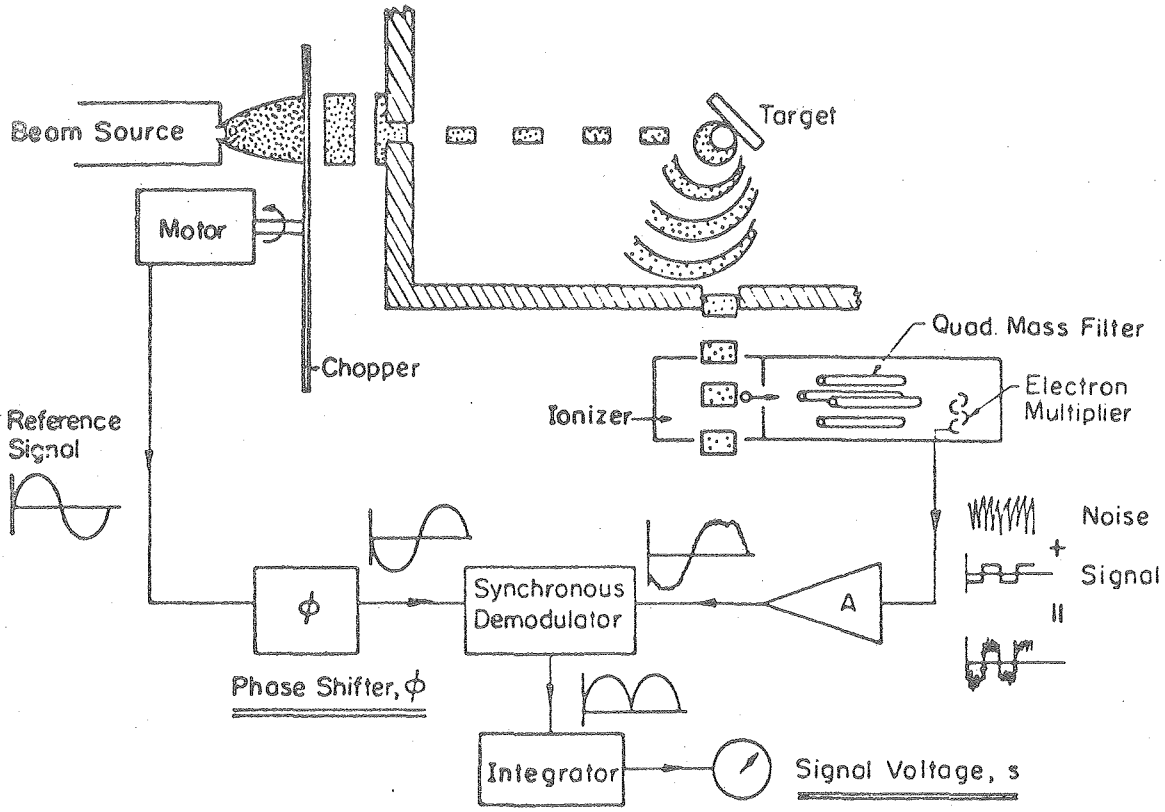

FIGURE 1 Schematic of modulated molecular beam apparatus for surface chemical kinetic studies

III Results

Data on the reaction was taken at varying UO_2 temperatures (320 °C - 1400 °C) and equivalent hydrogen pressures (1×10^{-5} torr - 5×10^{-4} torr). Most of the data were not consistently reproducible. Fig. 2 is a plot of the apparent reaction probability (which in the case of no beam modulation becomes the ratio of the number of H_2O molecules produced by the reaction to the number of H atoms incident on the target) versus reciprocal temperature of the UO_2. Three example data runs are shown on the plot as an illustration of the problem of obtaining consistent results.

IV Discussion

Possible troubles which could account for the anomalous results and the corresponding corrective action which has been taken fall into three catagories:

(1) Beam problems

(2) Sample problems

(3) Detector problems

A. Beam Problems

It was discovered that under certain conditions water vapor appears in the reactant hydrogen beam resulting in an erroneously high reaction probability reading. To correct this, the liquid nitrogen water trap was repositioned on the inlet gas line immediately before the source oven and after all junctions, valving, gauges, and non-bakable tubing. O-ring junctions were replaced with swagelock fittings and the pressure regulator on the hydrogen tank is being leak-tested to eliminate possible sources of H_2O contamination.

To ensure that the hydrogen beam is properly aligned with the UO_2 target, initial alignment is now checked mechanically by use of a fine wire temporarily inserted along the beam path prior to sealing the apparatus.

Fine tuning of the beam is accomplished under vacuum by manipulating the hydrogen source tube to peak the reflected hydrogen signal from the mass spectrometer.

B. Sample Problems

The UO_2 samples used were found to have a thin coating of sample holder material (molybdenum or tungsten) on the reaction face after high temperature experimentation. To prevent overheating of the sample holder due to poor thermal contact between the holder and the UO_2 target and resultant coating of the sample, graphite and molybdenum holders which firmly clamp the UO_2 target were fabricated. This sample holder design is shown in Fig. 3. A UO_2 sample with a tungsten coating chemically vapor deposited onto the rear of the sample is being prepared as a "back up." All UO_2 samples will be sintered at $\sim$ 1900 °C for several hours in a hydrogen atmosphere just prior to insertion into the apparatus. This should achieve uniform surface condtions by removing polishing debris and surface oxidation.

C. Detector Problems

The high-gain pulse electron multiplier was replaced with an electron multiplier optimized for the analog-type electronics used in our system (lock-in amplification). The pulse-type electron multiplier might possibly contribute to non linear analog response, (i.e. overloading of the front stage of the lock-in amplifier), under high gain, high count rate conditions.

Finally, deaterium will be used as a reactant in place of hydrogen. The lower mass spectrometer noise background at the D_2O (mass 20) peak compaired to the H_2O (mass 18) peak should allow measurement of lower reaction probabilities in less time with smaller error.

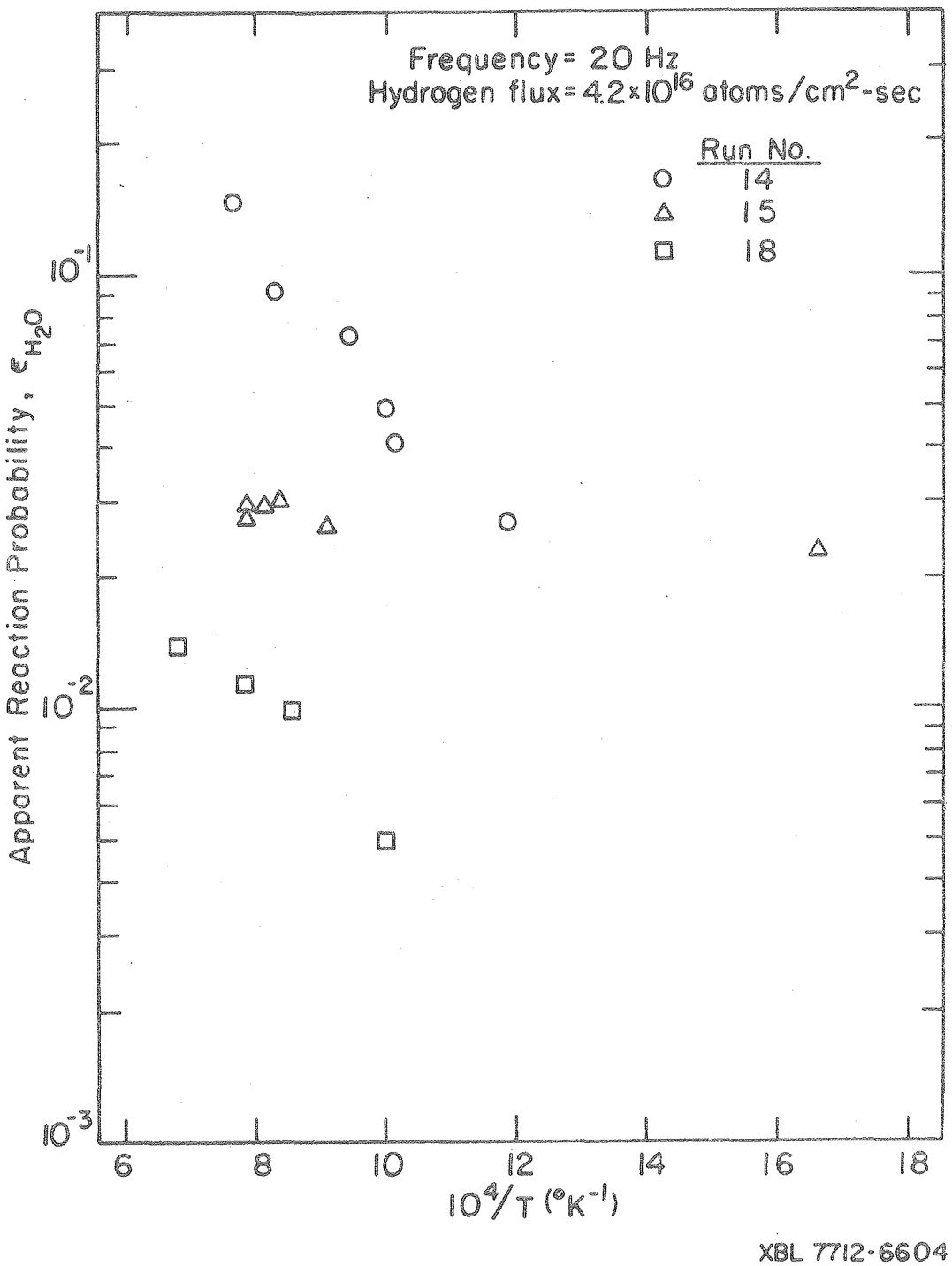

Fig. 2. Reaction probability of atomic hydrogen on UO_2.

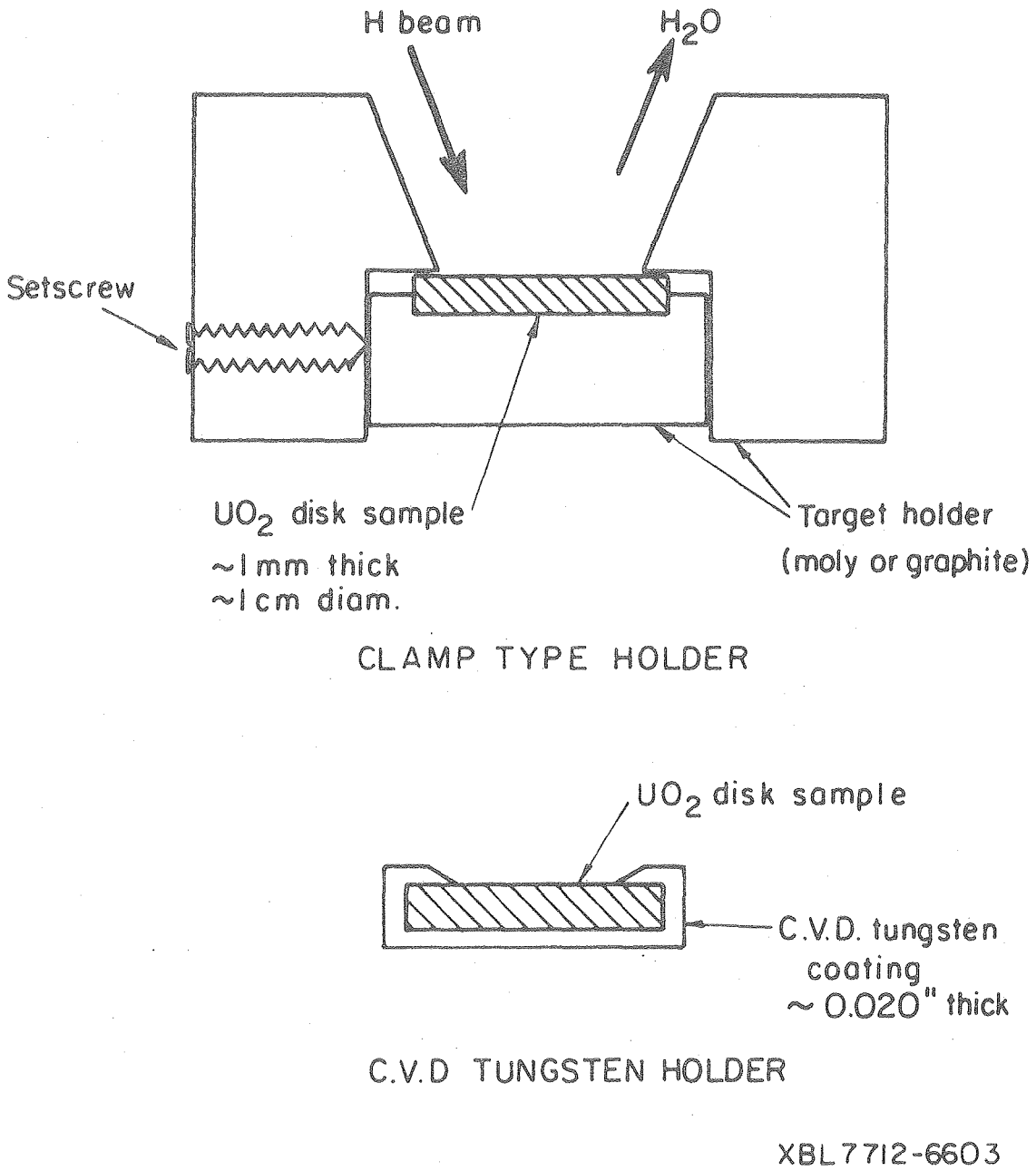

Fig. 3. UO_2 sample holders designed for good thermal contact.

V. Future Experiments

The present UO_2 samples under study are probably of a hyperstochiometric nature due to prolonged exposure to atmospheric oxygen and moisture. Future experiments will investigate the effect of changing oxygen-to-metal ratio upon reactivity by using both stochiometric UO_2 and hypostochiometric UO_2 polycrystalline wafers as targets. A single-crystal UO_2 target will also be studied to determine the effect of grain boundries and crystal orientation upon reactivity.

When the UO_2 experiments are complete, both polycrystalline Al_2O_3 (lucalox) and single-crystal Al_2O_3 (sapphire) will be used as targets.

References

1. D.M.Gruen, "Chemical Effects of Thermonuclear Plasma Interactions With Insulator and Metal Surfaces," J. Nucl. Mater. 53, 220 (1974).

2. J.W.Tester, R.C.Feber, and C.C.Herrick, Heat Transfer and Chemical Stability Calculations for Controlled Thermonuclear Reactor (CTR), USAEC Report LA-5328-MS (July 1973).

3. R.H.Jones, W.J.Siekhaus, J.A.Schwurz and D.R.Olander, "Investigation of Gas-Solid Reactions by Modulated Molecular Beam Mass Spectrometry," J. Vac. Sci. & Technol. 9, 1429 (1972).

4. D.R.Olander, "Heterogeneous Chemical Kinetics by Modulated Molecular Beam Mass Spectrometry," J. Colloid & Interface Sci. 58, 169 (1977).

A STUDY OF MASS TRANSFER AND REDUCTION OF UO_2

by Kim Kee

I. INTRODUCTION

Oxygen self-diffusion in hypostoichiometric heavy metal oxides is of importance in predicting the rate of oxygen redistribution and other physico-chemical processes occurring in an irradiated fuel pin. Although there have been many measurements of oxygen diffusion in ordinary oxides and in hyper-stoichiometric uranium dioxide (UO_{2+x}) (1), similar measurements in UO_{2-x} have proven very difficult — mainly because UO_{2-x} is a defect structure stable only at $T > 1300^{\circ}C$, and its oxygen diffusivity is likely to be large enough to render conventional methods unworkable (i.e., gas phase mass transfer or surface isotope exchange are rate-limiting). The method proposed involves a diffusion couple consisting of a UO_{2-x}^{18} wafer sandwiched to a UO_{2-x}^{16} wafer by a bond of liquid uranium. When heated, the O^{18} and O^{16} will interdiffuse. The hypostoichiometric samples are to be prepared by hydrogen reduction of UO_2 at high temperature:

$$UO_2 + xH_2 \rightarrow UO_{2-x} + xH_2O$$

The course of the reduction process will be followed by an electromicro-balance which continuously monitors the weight of sample. At high temperatures (~1900°C), however, the sample loses weight not only by reduction but also by vaporization of UO_2. Therefore, in order to study the reduction process, it is important to first characterize UO_2 vaporization in the flowing gas stream.

II. EXPERIMENTAL

Figure 1 shows the set-up of the furnace. The samples are suspended from the electromicrobalance by a rhenium wire. The gas is fed into the bottom of the tungsten crucible and flows upward. The crucible is heated by a tungsten mesh heating element from the outside. The temperature is

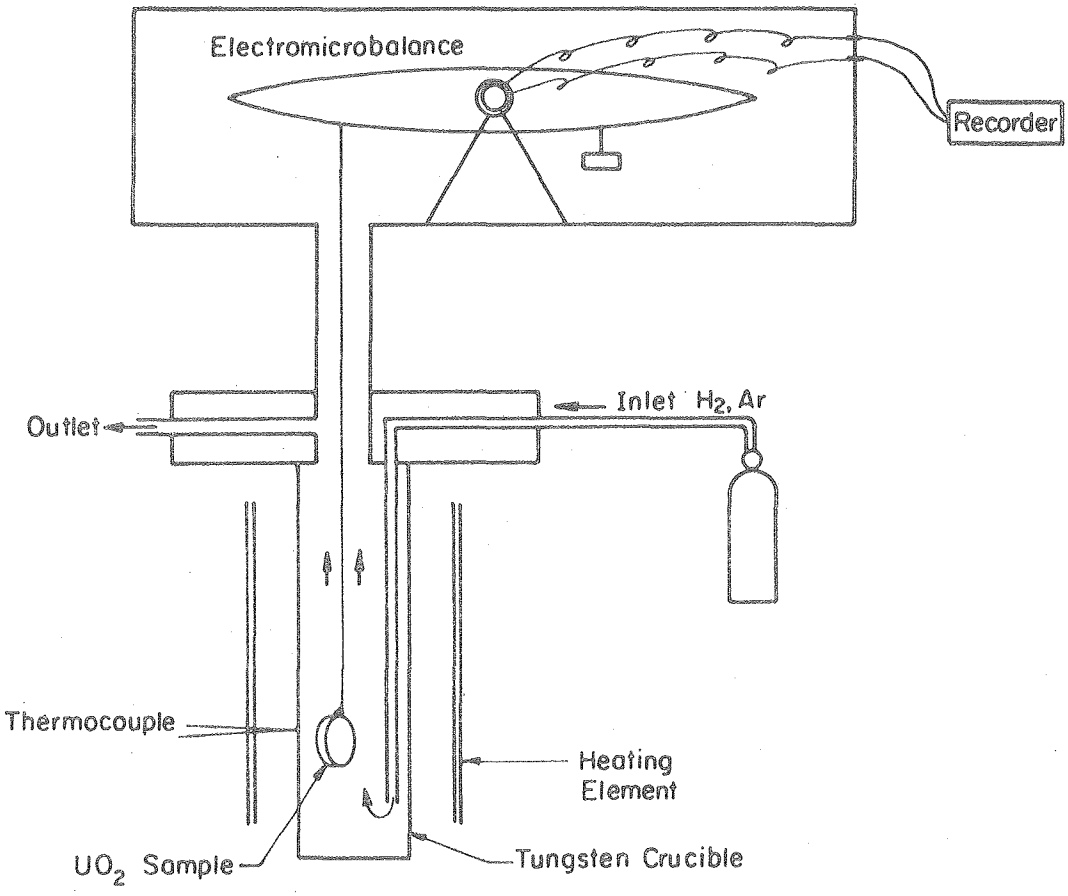

Fig. 1. Apparatus for investigating the kinetics of UO_2 vaporization or reduction in flowing gas streams at one atmospheric pressure.

measured by a tungstein-rhenium thermocouple external to the crucible at the sample position. The UO_2 wafers are 1 mm thick and 1.2 cm diameter. Also, iron samples of similar size were tested for the purpose of comparison. The vapor pressure of iron is well known (2). Argon and hydrogen were used for UO_2 and helium and hydrogen for iron. The weight loss rates were measured for different temperatures and for different gas flow rates.

III. RESULTS AND DISCUSSION

A. UO_2 Vaporization in Argon

Table 1 shows the weight loss rates of UO_2 in argon streams at three different temperatures and different flow rates.

TABLE 1. UO_2 vaporization in argon.

Data				Mass transfer coefficient (cm/sec)	
T (°K)	Flow Rate (cc(STP)/sec)	v (cm/sec)	$\dot{W}$ (mg/min)	k_m	k_m'
1840	20	18.8	$\cong 0$	0	--
2173	8	8.9	0.009 ±0.001	24.4	4.2
2173	10	11.1	0.010 ±0.001	27.1	4.7
2173	20	22.2	0.014 ±0.002	39.0	6.6
2273	20	23.3	0.048 ±0.005	38.0	7.0

T = temperature

v = velocity

$\dot{W}$ = weight loss rate

k_m = experimental mass transfer coefficient, defined by $J = k_m P_{eq}/RT$

k_m' = mass transfer coefficient calculated from theory

$Sh = k_m \ell / D$

$Sc = \nu / D$

ℓ = diameter of sample

D = diffusivity of UO_2 in Ar

P_{eq} = vapor pressure of UO_2

J = mass flux

$Re = v\ell/\nu$

ν = kinematic viscosity

From the analogy between heat and mass transfer laminar boundary layer theory for a flat plate, the mass transfer coefficient k_m can be predicted by: $Sh = 0.664\ Sc^{1/3}\ Re^{1/2}$. (1)

As can be seen in Fig. 2, mass transfer of UO_2 vapor in argon is as much as six times faster than predicted. Using least squares fitting, the data at 2173 K can be represented by: $Sh = 3.91\ Sc^{1/3}\ Re^{(0.47 \pm 0.01)}$. The possible errors may be: (i) underestimation of diffusivity of UO_2 in argon. The transport properties were estimated from theory (3) and are given in Table 2. (ii) Flat plate boundary layer theory is not very accurate for a thick disk hung in a gas stream. (The effect of decreasing flow path length from the center to the periphery is small.) However, the data still seem to follow the expected dependence on Reynolds number, as shown in Fig. 2.

TABLE 2. Diffusivity and viscosity of Ar and H_2.

T (°K)	$D_{UO_2\text{-}Ar}$ (cm^2/sec)	μ_{Ar} (poises)	$D_{UO_2\text{-}H_2}$ (cm^2/sec)	μ_{H_2} (poises)
2073	2.31	7.7×10^{-4}	12.53	3.2×10^{-4}
2173	2.48	7.8×10^{-4}	13.59	3.3×10^{-4}
2273	2.71	7.9×10^{-4}	14.54	3.4×10^{-4}

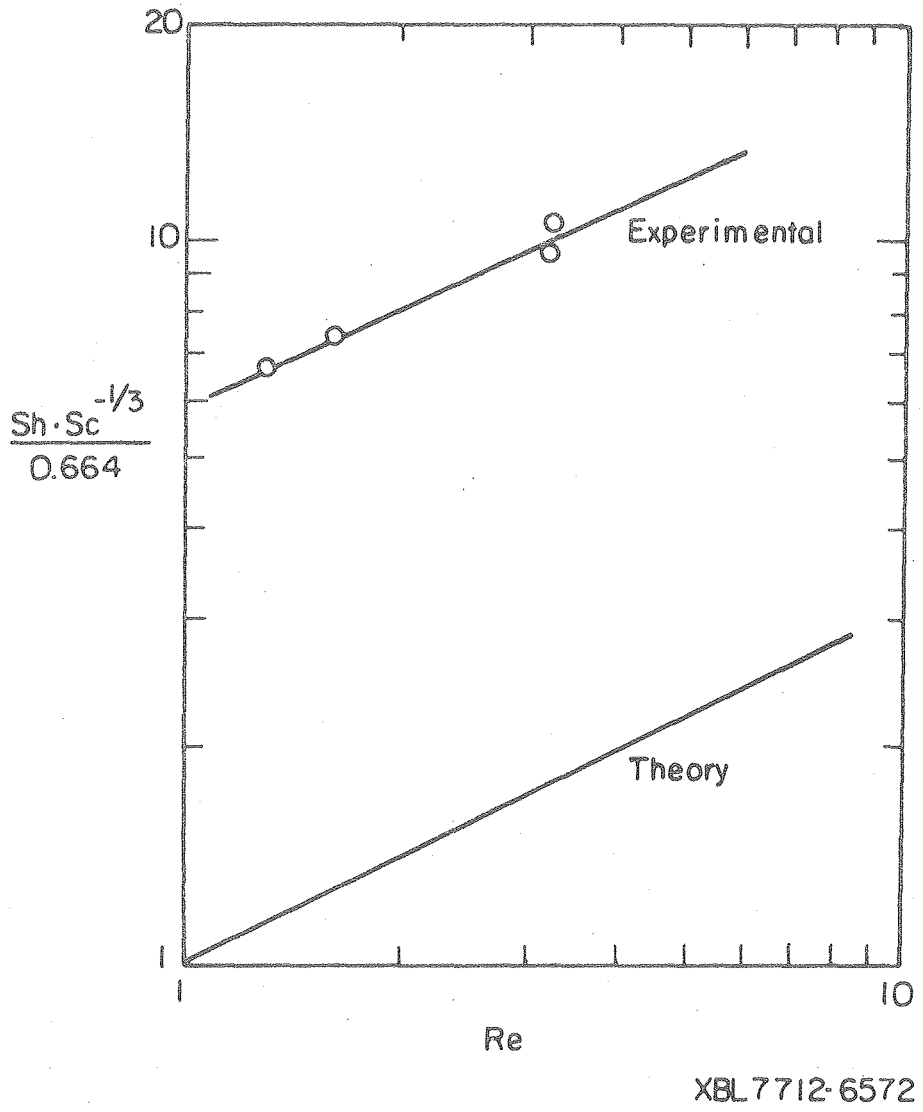

Fig. 2. Comparison of UO_2 vaporization in argon with flat plate boundary layer theory for Reynolds number variations.

The effect of temperature on UO_2 vaporization can be estimated from the data in Table 1 at 2173 K and 2273 K. From Eq. (1) and $J = k_m \frac{P_{eq}}{RT}$, and $\dot{W} = JA$, where A = surface area of sample,

$$\frac{\dot{W}}{A} = k_m \frac{P_{eq}}{RT} \qquad \text{or} \qquad \frac{\dot{W}T}{DSc^{1/3}\,Re^{1/2}} \propto P_{eq} .$$

In Fig. 3, the temperature dependence of $\frac{\dot{W}T}{DSc^{1/3}\,Re^{1/2}}$ is compared with equilibrium vapor pressure curve. Again, using least square fitting gives a slope corresponding to a heat of vaporization $\Delta H_{vap} = 123.3 \pm 4.5$ kcal/mole, which is comparable to $\Delta H_{vap} = 143.1$ kcal/mole from the equilibrium vapor pressure curve (4).

B. UO_2 Reduction in Hydrogen

Table 3 shows the results in a hydrogen stream:

TABLE 3. UO_2 reduction in hydrogen.

T (°K)	Flow rate (cc(STP)/sec)	$\dot{W}$ in H_2 (mg/min)	$\dot{W}$ in Ar (mg/min)	Expected $\dot{W}$ in H_2 (mg/min)
2173	10	0.011 ±0.0005	0.010 ±0.001	0.021
2173	20	0.050 ±0.0025	0.014 ±0.002	0.029

Figure 4 is a typical weight loss curve in which one can see the sharp change of the slope after the argon stream was switched to hydrogen.

Also shown in Table 3 are the weight loss rate of argon for comparison. Using Eq. (1), the ratio of k_m in H_2 to that in Ar is estimated to be ≅2.1 at the same temperature and flow rate, and the weight loss rates due to pure evaporation are listed as "Expected $\dot{W}$ in H_2" in the table. However, the data at a flow rate of 10 cc/sec show a slower rate than expected, especially considering the contribution of reduction. This is believed to be experimental error. Another possibility is that the rate 0.011 mg/min

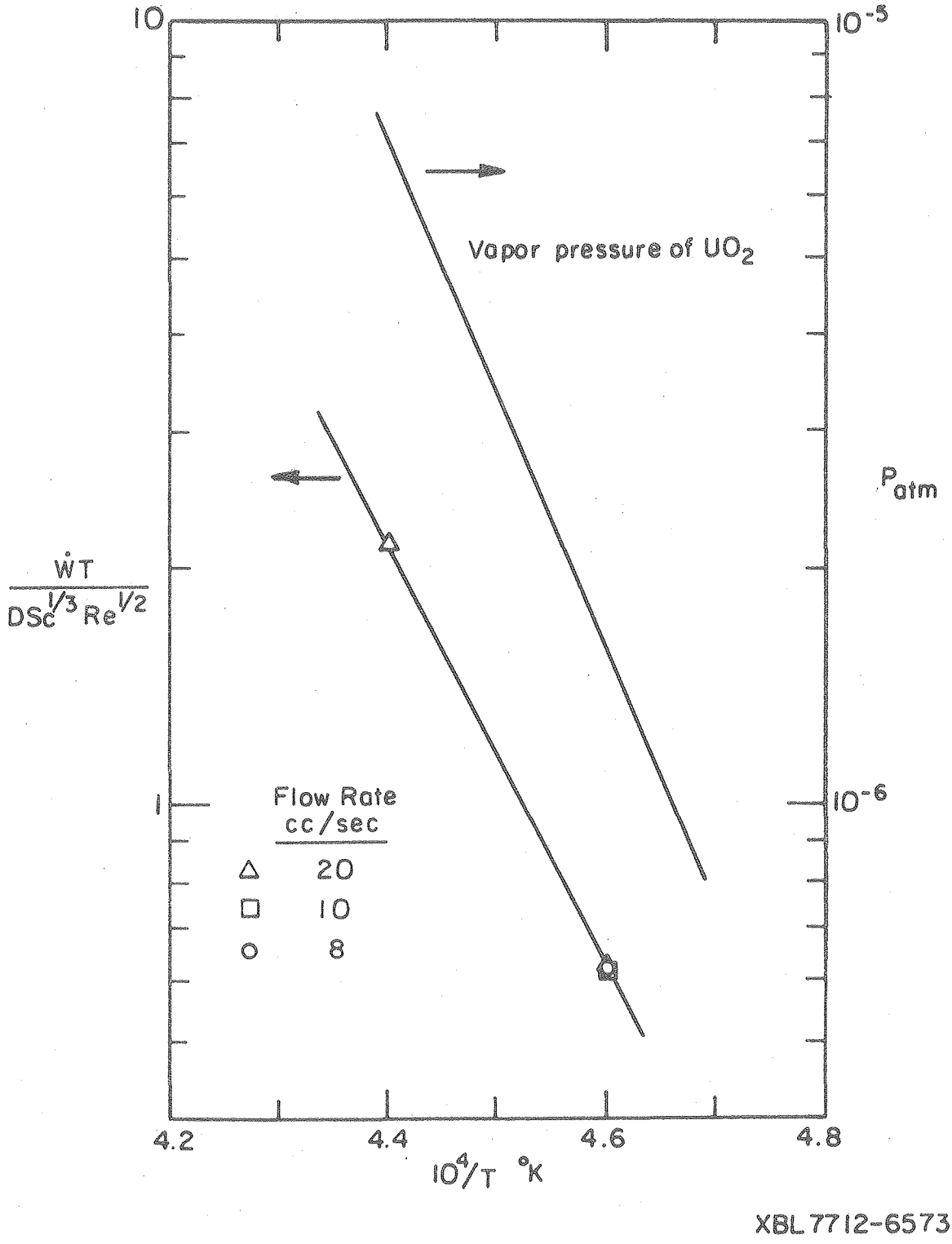

Fig. 3. Temperature dependence of the UO_2 vaporization rate.

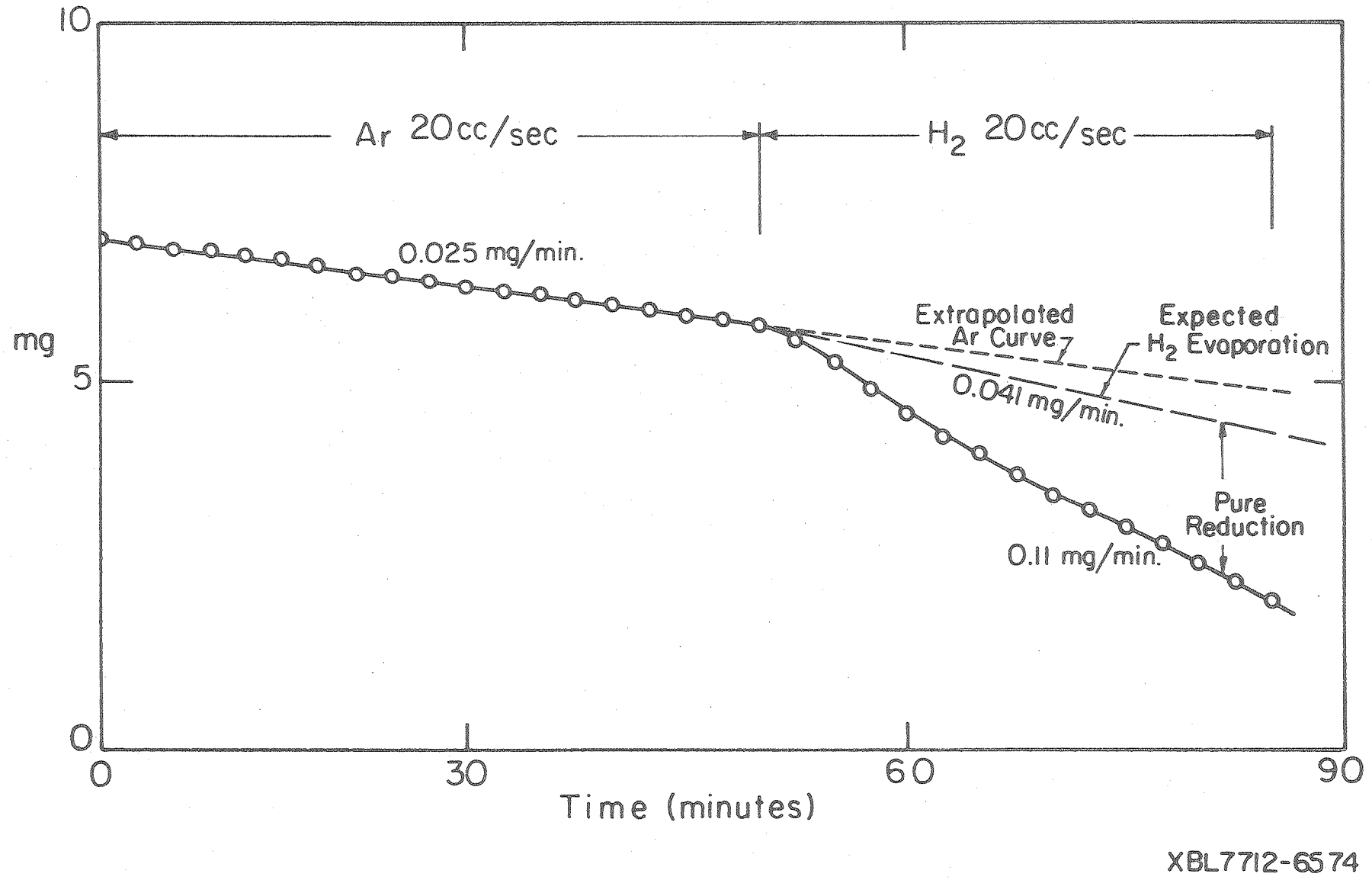

Fig. 4. Typical weight loss data for UO_2 in flowing argon and hydrogen.

was measured before steady state was reached. For a flow rate of 20 cc/sec, if the data are accurate, the weight loss rate 0.050 - 0.029 = 0.021 mg/min can be attributed to the reduction of UO_2 by H_2. At this rate, UO_2 can be reduced to $UO_{1.977}$ in an hour, assuming that the vapor pressure is independent of stoichiometry within this range. This rate of reduction is significant and may even be mass transfer-limited (rather than limited by surface chemical reaction or solid-state diffusion of oxygen in the UO_{2-x}).

C. Iron Vaporization

Iron evaporation results are shown in Table 4 (following page).

Figure 5 shows that mass transfer is 2 to 3 times higher than expected from the theory. Using least square fitting, the experimental data can be represented as: $Sh = 0.8\ Sc^{1/3}\ Re^{(0.115\ \ 0.3)}$. Diffusivities of Fe in H_2 and He are tabulated below:

Table 4. Diffusivity and viscosity of He and H_2.

T (°K)	D_{Fe-H_2} (cm^2/sec)	D_{Fe-He} (cm^2/sec)	μ_{H_2} (poises)	μ_{He} (poises)
1693	14.48	13.76	2.7×10^{-4}	6.3×10^{-4}
1773	15.75	14.88	2.9×10^{-4}	6.5×10^{-4}

The dependence of the Sherwood number on the Reynolds number does not agree with the value of 0.5 predicted by laminar flat plate boundary layer theory. This may be due to the sensitivity of the hydrodynamics to slight misalignment of the hanging specimen from the vertical axis. Note also that the magnitude of the discrepancy between theory and experiment is a factor or ~2 instead of ~6 for UO_2.

The heat of vaporization $\Delta H = 91.2 \pm 32.1$ kcal/mole was obtained from Fig. 6, which is comparable with $\Delta H = 90.1$ kcal/mole from the equilibrium vapor pressure curve (2).

TABLE 4. Fe vaporization in H_2 and He.

T (°K)	P_{eq} (atm)	Flow (cc(STD)/sec)	v (cm/sec)	$\dot{W}$ in H_2 (mg/min)	k_m (cm/sec)	k_m'	W in He (mg/min)	k_m	k_m'
1486	--	20	13.96	0	--	--	--	--	--
1693	1.21×10^{-5}	10	7.95	--	--	--	0.012 ± 0.003	22.9	9.1
1693	1.21×10^{-5}	20	15.9	0.013 0.004	24.8	13.63	0.013 ± 0.002	24.8	12.9
1773	4.12×10^{-5}	5	4.16	0.038 0.008	22.2	3.64	--	--	--
1773	4.12×10^{-5}	10	8.33	0.038 0.007	22.2	7.30	0.030 ± 0.005	17.5	9.3
1773	4.12×10^{-5}	20	16.65	0.041 0.005	23.6	14.59	0.039 ± 0.002	22.8	13.6

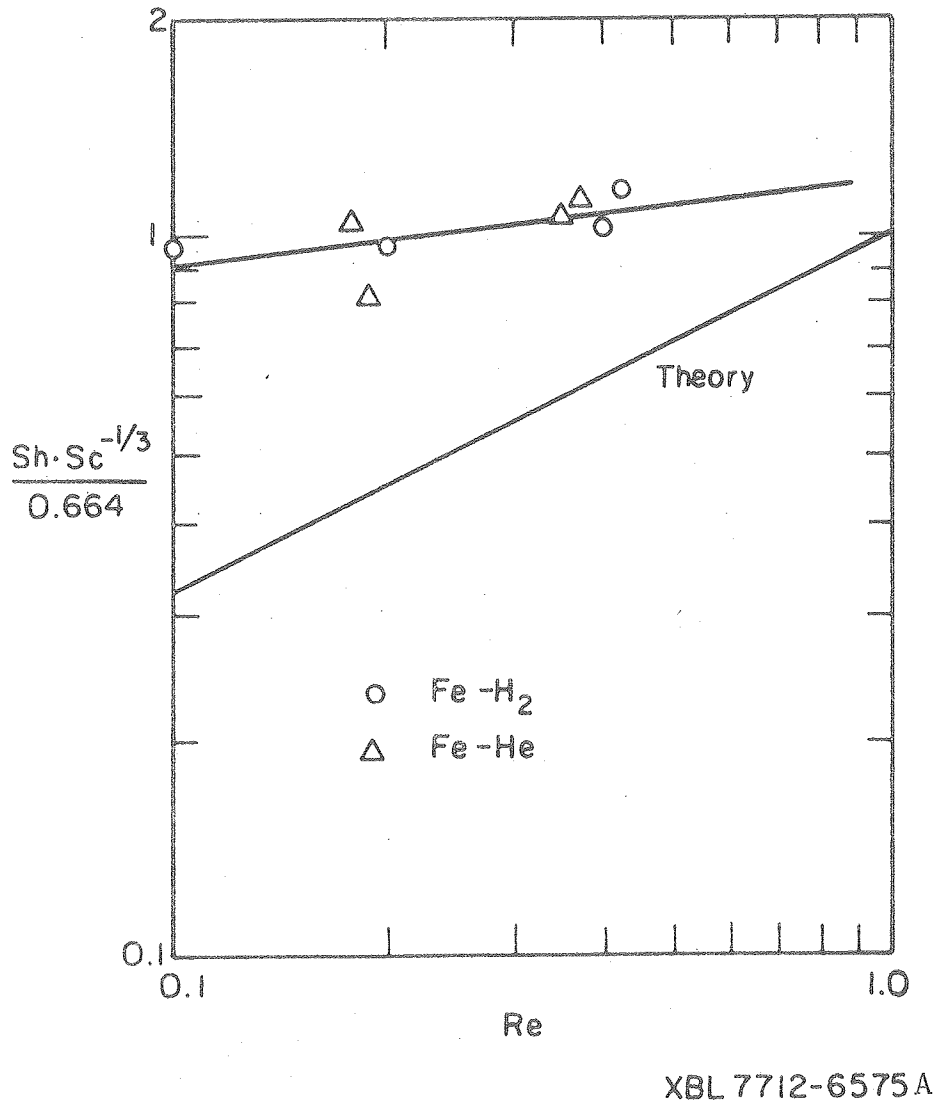

Fig. 5. Comparison of iron vaporization in hydrogen and in helium.

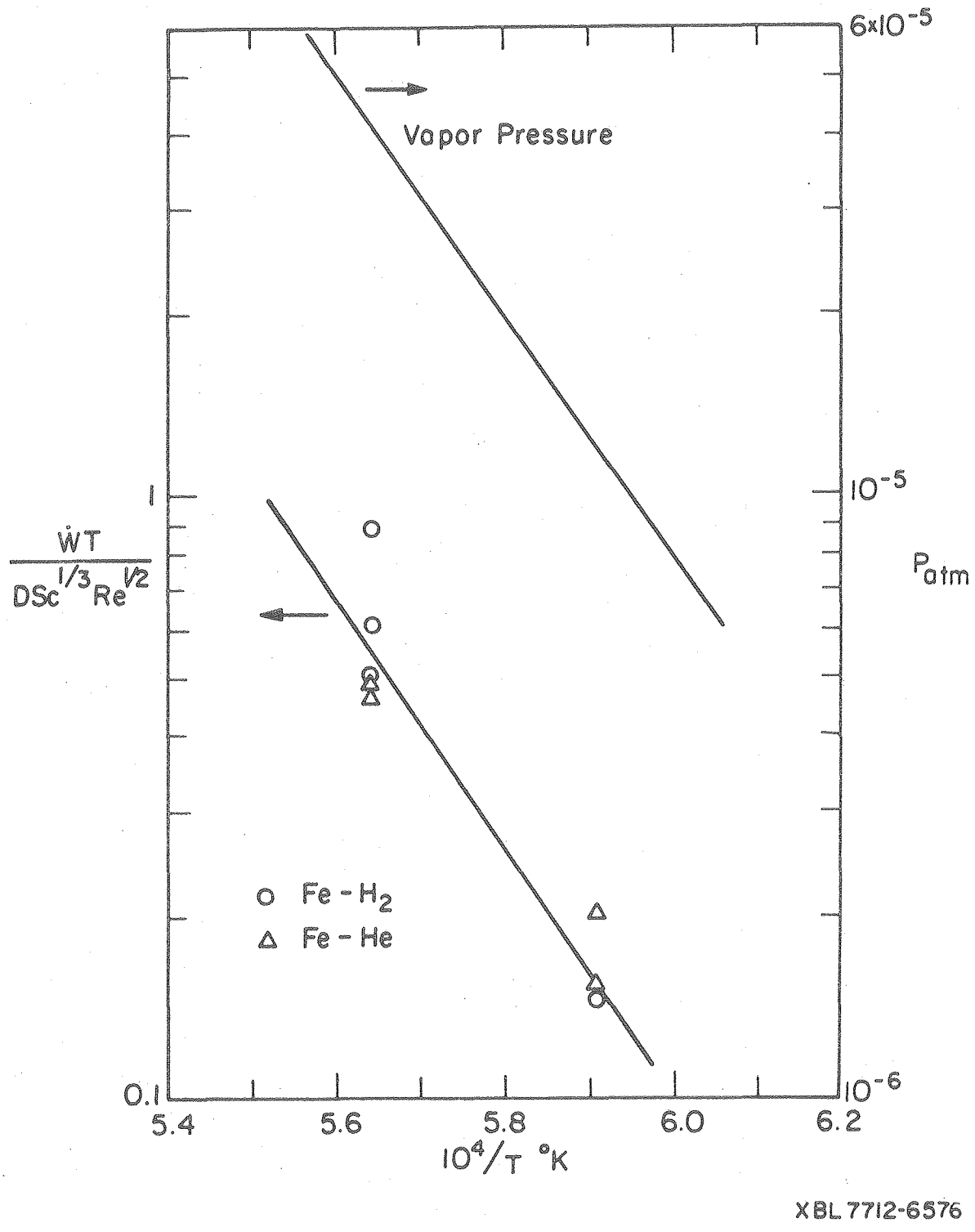

Fig. 6. Temperature dependence of iron vaporization.

IV. FUTURE PLANS

Studies on stoichiometry determination will be continued. UO_2^{18} will be made from UO_2^{16} using a controlled atmosphere of H_2O^{18}/H_2. Interfacial contact between liquid uranium metal and UO_{2-x} will be studied, and hopefully, diffusion couples will be successfully fabricated.

References

1. J.F.Martin and P.Contamin, J. Nucl. Mater. 30, 16 (1969).

2. A.N.Nesmianov, Vapor Pressure of Chemical Elements, edited by R.Gary (Elsevier Publishing Co., Amsterdam, 1963).

3. R.C.Reid and T.K.Sherwood, The Properties of Gases and Liquids, 2nd edition, (McGraw-Hill Book Co., New York, 1960), pp.523-25.

4. M.Tetenbaum and P.D.Hunt, J. Nucl. Mater. 34, 86 (1970).

THE KINETICS OF LASER PULSE VAPORIZATION OF UO_2

by C. H. Tsai

I. Introduction

Safety analysis of nuclear reactors requires knowledge of the equation of state (i.e., the vapor pressures of all species) and the evaporation kinetics of the fuel material at temperatures well above the melting point (1). Current reactor disassembly analyses rely on the direct extrapolation of low temperature data or calculations based on some theoretical models (1-6). Fig. 1 shows some of the direct extrapolations which account only for the heat of fusion at melting point. The extrapolation to 5000 K leads to orders-of-magnitude uncertainty in fuel vapor pressure because of the disagreement of the various low temperature measurements, which is greatly magnified by the strong dependence of the vapor pressure on temperature (i.e., the large heat of vaporization of UO_2). Moreover, the extrapolated vapor pressure - temperature curves are based on the assumptions that (a) thermodynamic equilibrium exists between the vapor phase and the fuel melt and (b) the hot fuel retains its original composition while evaporating. In view of the questionable validity of these two assumptions and the necessity of large data extrapolation even if they are, experimental determination of the vapor pressures and evaporation kinetics of fuel material in temperature range up to 5000 K is essential.

At extreme temperatures, conventional vapor pressure measurement techniques fail not only because of a lack of high melting crucible material, but because of a departure from free molecule evaporation. Molecular evaporation can only be maintained by heating the surface in a pulsed mode and restricting the heated area to a very small spot. Laser heating technique has been developed recently to enable attainment of ultra-high temperatures within an extremely small spot during a short pulse and to

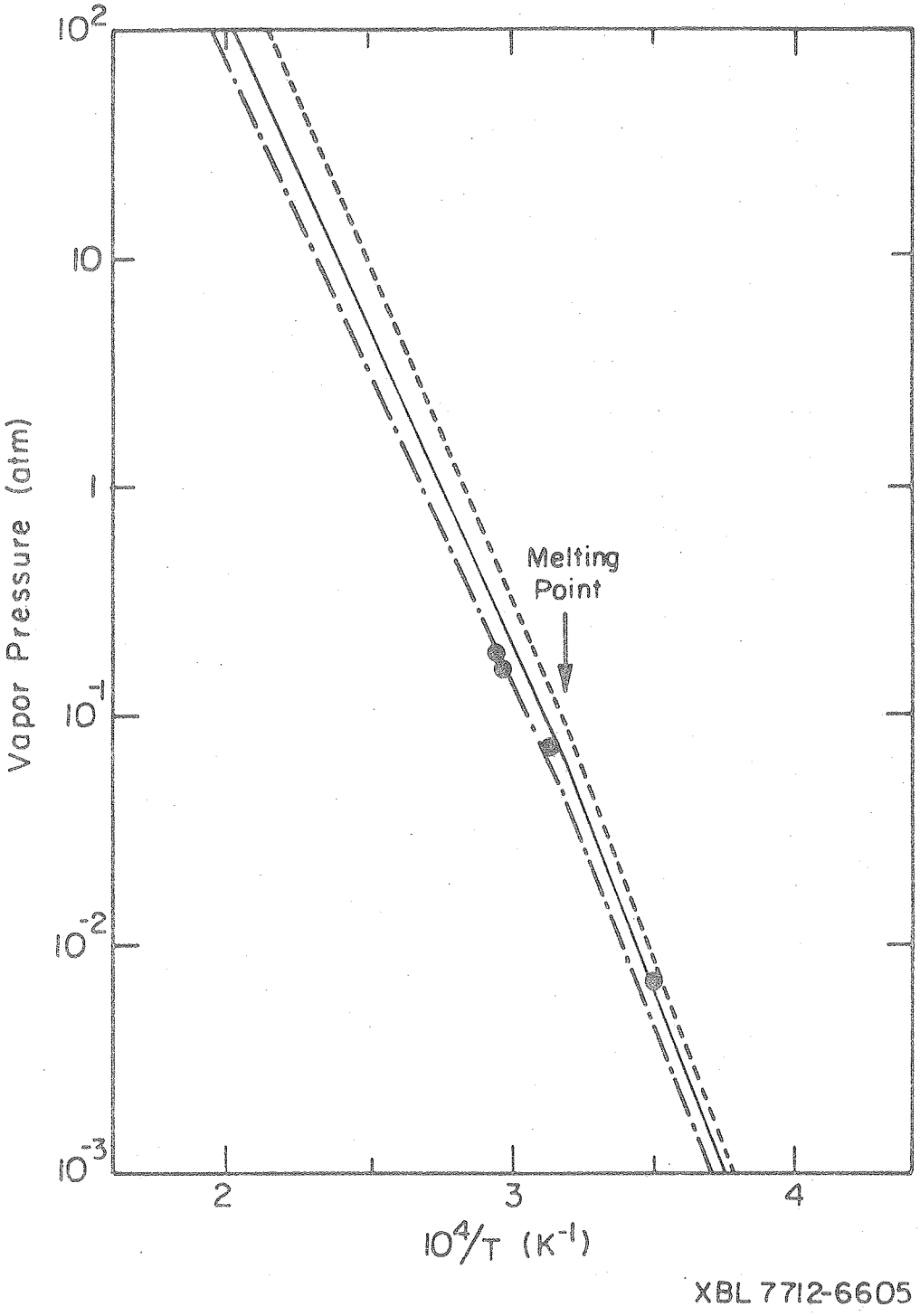

Fig. 1. Total vapor pressure of UO_2 by direct extrapolation of low temperature data; ------- from Ohse (15); — · — · — from Tetenbaum and Hunt (16); ———— is averaged; and the dots are from Reedy and Chasanov (3).

simulate the evolution of the temperature excursion in a reactor accident. The hypothetical prompt critical accident which causes extensive fuel evaporation is characterized by:

- temperatures between 4000 and 5000 K,
- evaporation times in the millisecond range and
- surface recession velocities between 1 and 100 cm/s.

Two German groups (7-10) and a Japanese laboratory (11) have been attempting to develop the laser pulsing measurement by different approaches. However, their results are still subject to considerable uncertainties. Our experiments utilize two independent laser pulsing measurement: (a) a photographic technique and (b) a mass spectrometry method for vapor species identification. The experiments utilizing the photographic method are conducted jointly by LBL and NASA personnel (A. Covington and K. Lincoln) at the laser facilities of NASA Ames Laboratory.

II. Theory

With the conventional measuring methods (useful up to 3400 K), the composition of the evaporating surface is maintained during the evaporation process. In the laser pulsing techniques, however, the high evaporation rates change the composition of the evaporating surface, giving the vapor pressures which are different from the equilibrium pressures. Such types of evaporation are also to be expected in loss-of-coolant reactor accidents.

A computer code similar to that of Breitung (5) but with the full transient property accounted for has been developed at LBL. The code calculates the surface temperature and surface composition of uranium oxide target during the laser evaporation transient by simultaneously solving the one-dimensional heat conduction equation and the oxygen diffusion equation. Equilibrium free-molecule evaporation is assumed.

III. Photographic Method

(a) Experimental:

A sketch of the NASA Ames experimental apparatus is shown in Fig. 2. The solid is laser-pulsed in an ambient insert gas in order to develop the visible shock structure. A conventional camera is used to obtain time-integrated images of the evaporating UO_2 free-jet structure and the total vapor pressure is interpreted from the Mach disk formula by analogy with a free jet from a sonic orfice (12). The barrel shock wave and the normal shock (or Mach disk) appear as well-defined boundaries on the photos. The maximum displacement of the standing shock from the vaporizing surface (i.e., the position of the outer boundary of the Mach disk) corresponds to the time at which peak surface temperature and pressure occur. It has been found that the Mach disk location can be correlated by the empirical relation (12):

$$x/D = 0.67(P_o/P_1)^{1/2} \qquad (1)$$

where x is the axial distance between the Mach disk and the orifice, D is the orifice diameter, P_o is the total reservoir pressure, and P_1 is the ambient pressure.

In applying Eq. (1) to laser pulsing of solids, the following identifications are made (13):

(i) the "orifice" is the spot on the solid illuminated by the laser

(ii) the "reservior pressure" is the vapor pressure at the maximum temperature of the solid surface.

Fig. 3 shows a typical surface temperature trace from a wide-band silicon photodetector pyrometer. Fig. 4 shows a typical photograph of the UO_2 vapor plume structure.

(b) Results:

The predictions of the computer code described in Sec. II are compared with the results from photographic experiments in Table I.

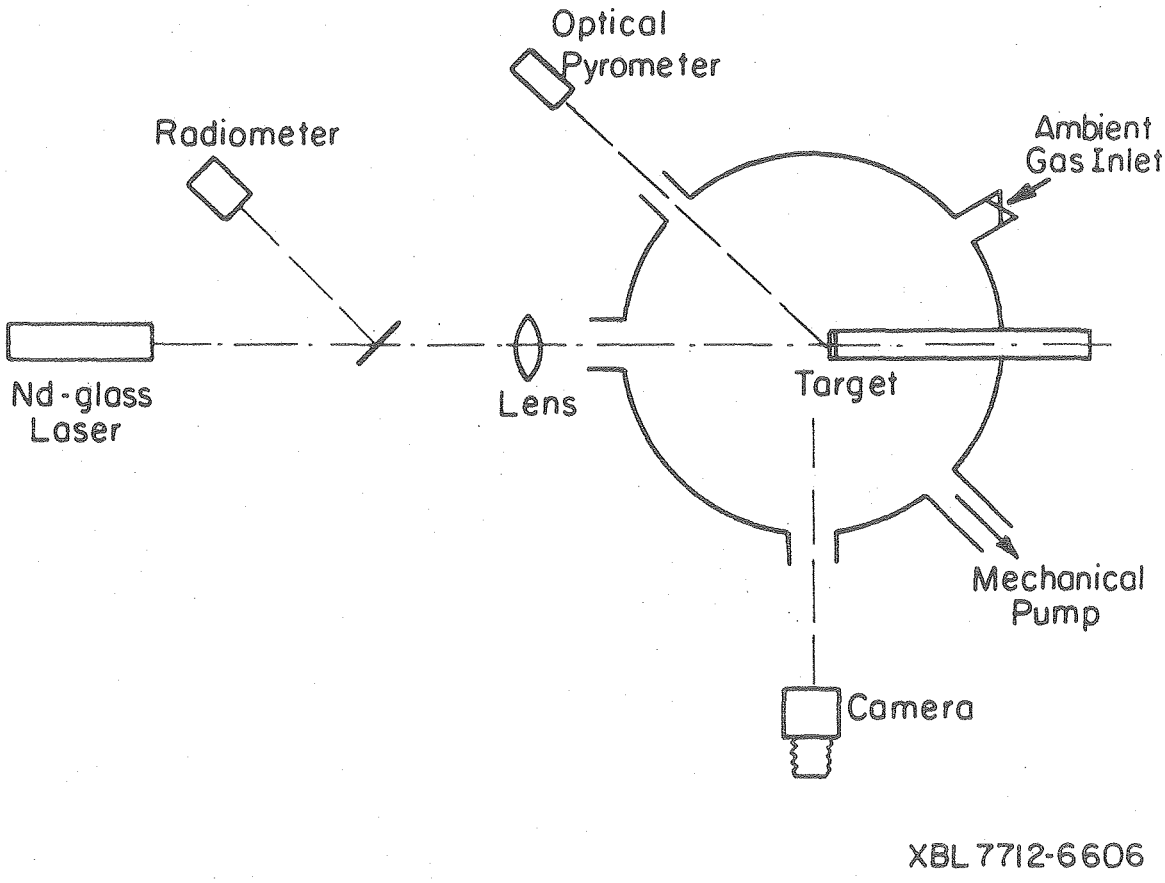

Fig. 2. The experimental apparatus for photographic measurements at NASA Ames Laboratory.

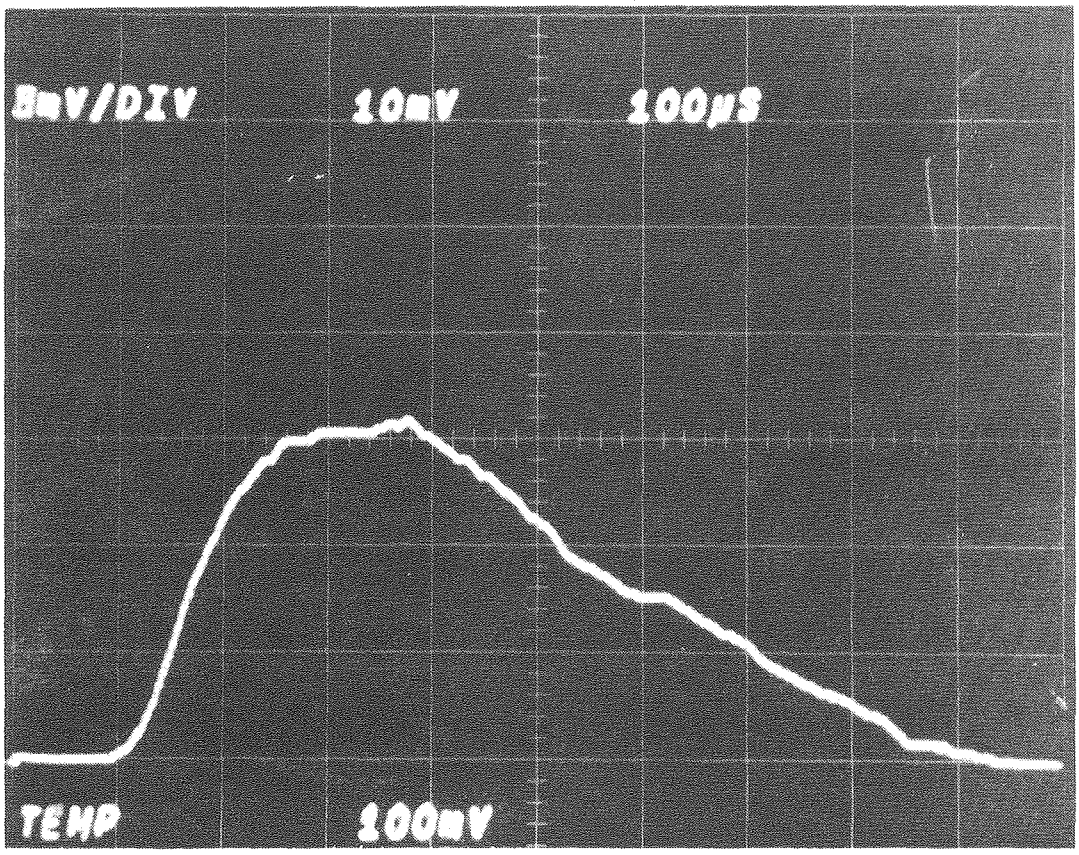

XBB 770-12667

Fig. 3. Typical picture of temperature trace from optical pyrometer.

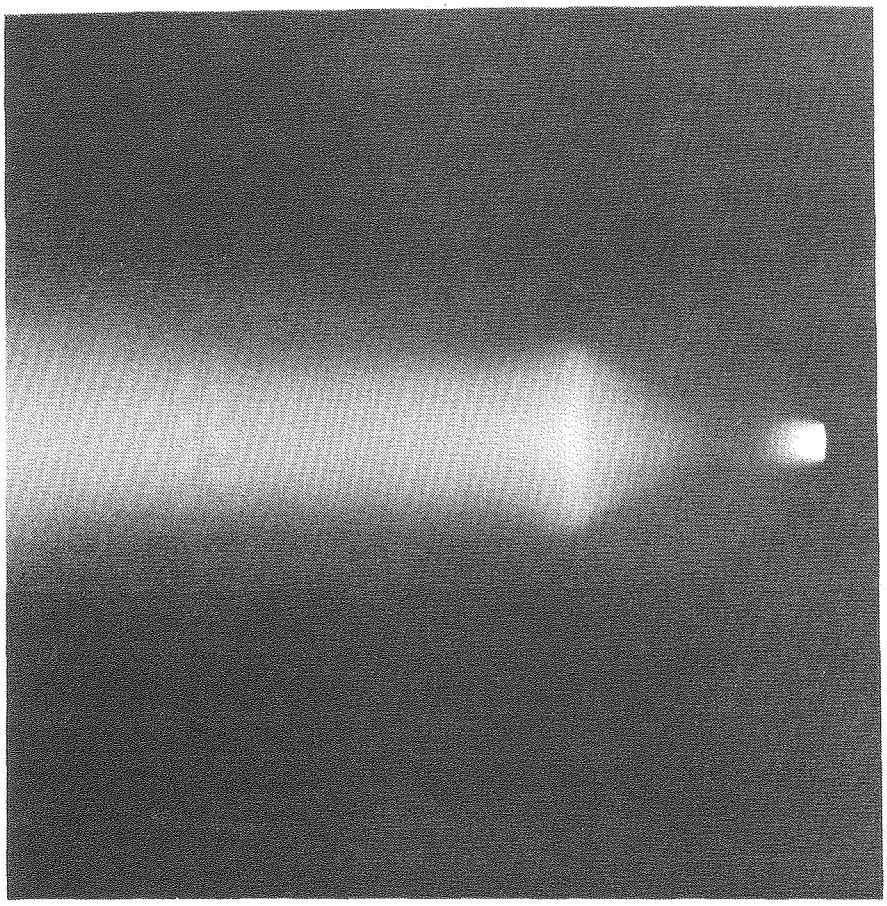

XBB 770-12666

$$\frac{X}{D} = 0.67 \left(\frac{P_o}{P_1}\right)^{1/2}$$

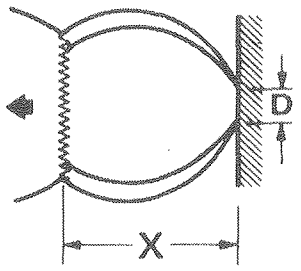

Fig. 4. Typical photograph of UO_2 vapor plume structure.

TABLE I. The experimental and calculated maximum surface temperatures and total vapor pressures for UO_2 on the NASA Ames apparatus.

Shot number	Energy of laser, Pulse E_i (J)	Peak power density ($10^5 W/cm^2$)*	Maximum temperature T_{exp} (K)	Maximum temperature T_{calc} (K)†	O/U† at max. temp.	Vapor pressure (atm) P_{exp}	Vapor pressure (atm) P_{calc}†
47	3.65	0.60	3396	3390	1.976	0.16	0.22
50	4.49	0.74	3643	3640	1.958	0.38	0.54
53	4.90	0.81	3755	3730	1.948	0.48	0.75
55	6.78	1.12	3984	3980	1.896	0.74	1.5
61	17.53	2.89	4926	4690	1.337	2.1	6.2
67	38.71	6.39	5764	5250	1.333	3.2	13.0
68	43.83	7.24	5917	5290	1.110	3.6	13.8

* Peak power density is given by $Q_p = \frac{P_{max}(1-R)}{A}$,

where P_{max} = peak power = $E_i/5.074 \times 10^{-4}$,
R = reflectivity of UO_2 to Nd-glass laser light = 0.95,
A = evaporation area = 0.113 cm^2.

† From computer code, allowing for oxygen depletion at the surface. The pressure is that at the maximum temperature of all uranium-bearing species over UO_{2-x}, where 2-x is the O/U ratio of the surface at the time of the maximum temperature.

The total energy of laser pulse and its temporal shape are obtained from the radiometer signal. The peak power density is obtained by dividing the peak power by the evaporation area assuming that the laser intensity is radially uniform. This information is then used as the input for the computer code to calculate the maximum surface temperature, the surface composition at the time when surface temperature is maximum, and the equilibrium vapor pressure corresponding to this temperature and O/U ratio.

Fig. 5 shows that the measured maximum surface temperature is greater than the temperature calculated from the computer code for the temperatures higher than 3900 K, and the discrepency increases with the temperature. The temperature calculation is not absolutely reliable because the high temperature properties of liquid UO_2 (e.g. heat capacity, thermal conductivity, oxygen diffusivity, emissivity, etc.), are not well established. Also, the temperature measured by optical pyrometry is expected to be larger than the actual temperature due to the optical absorption of laser radiation by the vapor plume, which increases with temperature. The excited gaseous UO, UO_2, and UO_3 emit radiation in the infrared which is detected by the wide-band pyrometer used in the NASA Ames apparatus. This emission has been observed spectroscopically, and contributes to the energy received by the pyrometer, thereby making the experimental temperature larger than that due solely to thermal radiation from the solid surface. However, in Fig. 6, the measured pressures plotted against the calculated temperature (which eliminates this experimental problem) still show a factor of 1.4 to 4 deviation from the predicted vapor pressure curve, even with surface composition depletion taken into account. This suggests that besides the uncertainty in temperature measurement, the pressure interpretation required in the Mach disk model might also have contributed to the discrepancy. The uncertainty might be due either (a) to incorrect measurement of equivalent

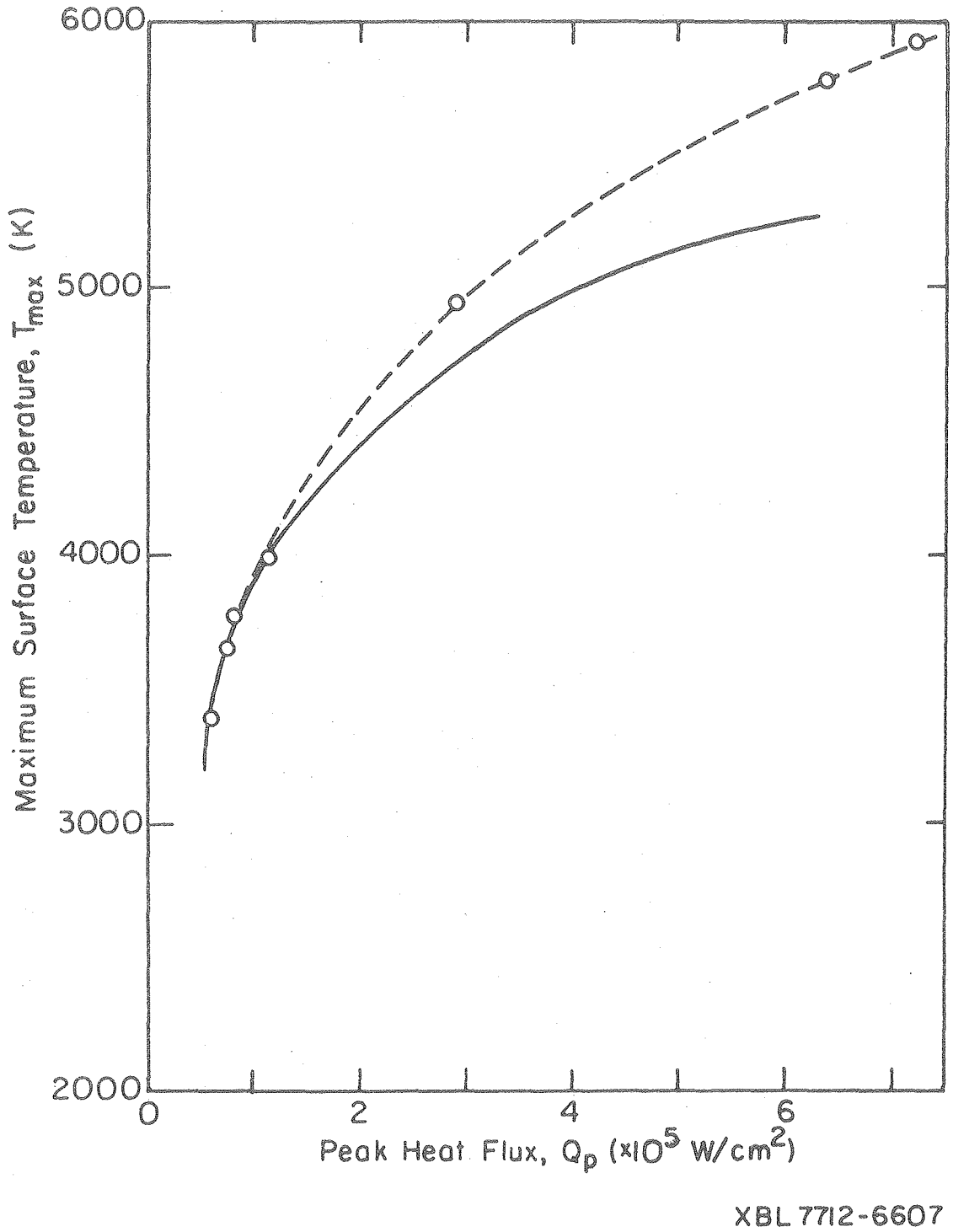

Fig. 5. Comparison of calculated and experimental maximum surface temperature. Solid line is calculated from computer code considering surface composition depletion; dashed line with hollow circles are the experimental results from NASA Ames apparatus.

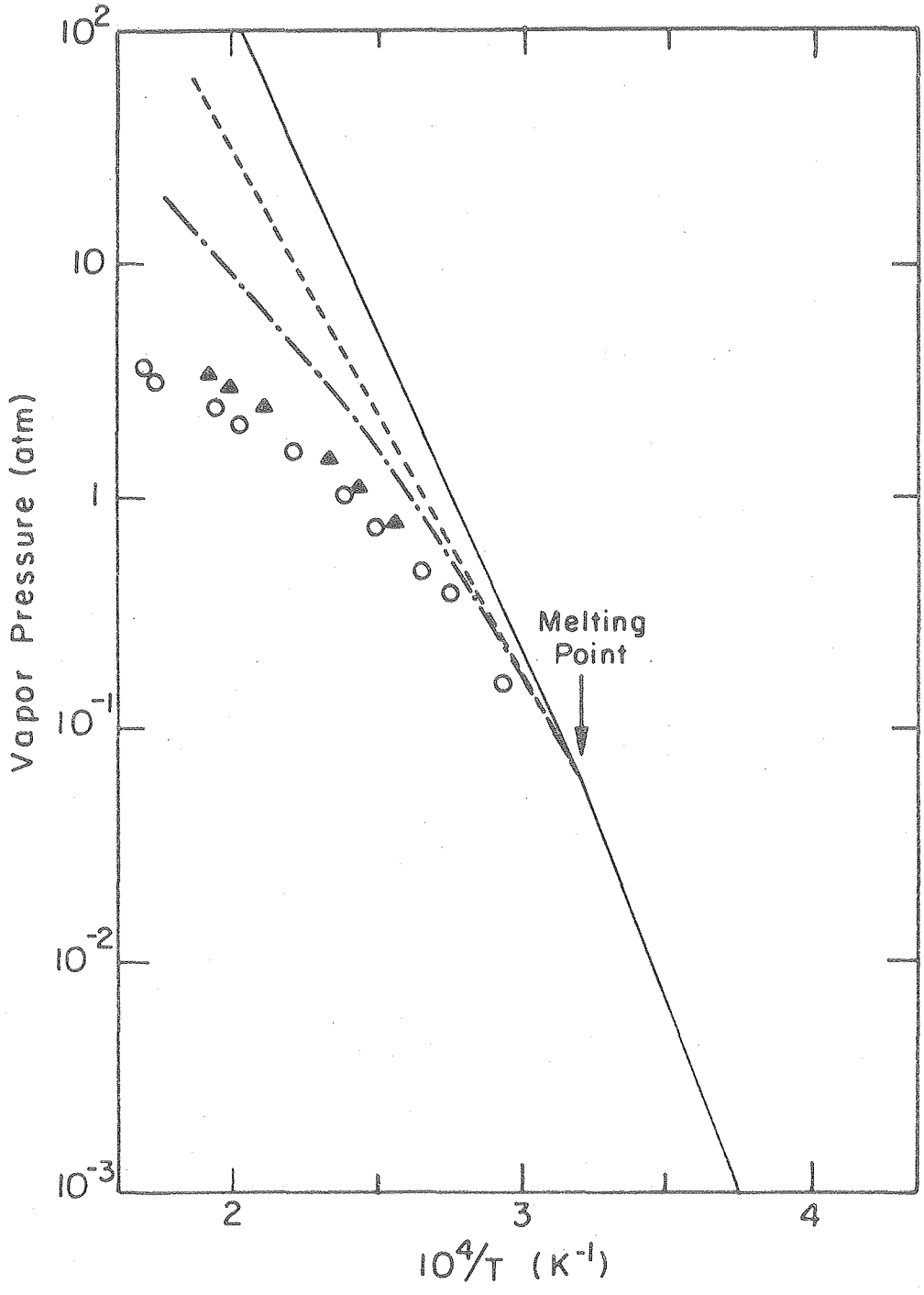

XBL 7712-6608

Fig. 6. UO_2 total vapor pressures; solid line is extrapolated data from Refs. 15 and 16 (averaged); dashed line is total vapor pressure of $UO_{2.00}$ from ROOT (17); dash-dot-dash is predicted vapor pressure including surface depletion; hollow dots are experimental data from NASA Ames apparatus; and solid triangles are experimental results, but with measured temperature replaced by calculated temperature.

"sonic orifice diameter" (which has been taken as the visible laser spot size) due to radial nonuniformity of the laser intensity profile, or (b) to the pressure drop across the hypothetical hydrodynamically non-equilibrium layer of a few mean free paths from the target surface - according to Anisimov's calculations (14), the reflux of vapor molecules to the surface due to gas phase collisions in the dense-gas plume is about 18% of the flux in the absence of collisions. In addition, the theory predicts a "reservoir" pressure adjacent to the solid surface about five times smaller than the saturation vapor pressure at the solid surface temperature. Also shown in Fig. 6 are direct linear extrapolations of the averaged vapor pressure - temperature equations of Ohse (15) and Tetenbaum & Hunt (16) and total equilibrium vapor pressure of stoichiometric $UO_{2.00}$ calculated from a subroutine developed by Blackburn (17) to correlate the thermochemistry of $UO_{2\pm x}$.

IV. Mass Spectrometric Method

Another UO_2 laser-pulsing measurement in the same temperature range which utilizes mass spectrometry is being conducted at LBL. A sketch of the experiemtnal set up is shown in Fig. 7. The solid is laser-pulsed in vaccum to permit in-flight detection of vapor species, which yields the vaporization rates and molecular velocities.

Mass spectrometry has the advantage of being able to detect individual vapor species and to obtain the information on partial vapor pressures rather than only the total vapor pressure measurable by the photographic method. Knowledge of vapor composition may reveal non-equilibrium behavior not available from the total vapor pressure (e.g., UO_3/UO_2 and UO_2/UO ratios). Chemical non-equilibrium has been observed in the laser pulsing of ZrH_2 (18). However, this determination is hampered by insufficient knowledge of the absolute ionization cross sections and fragmentation potentials of various vapor species.

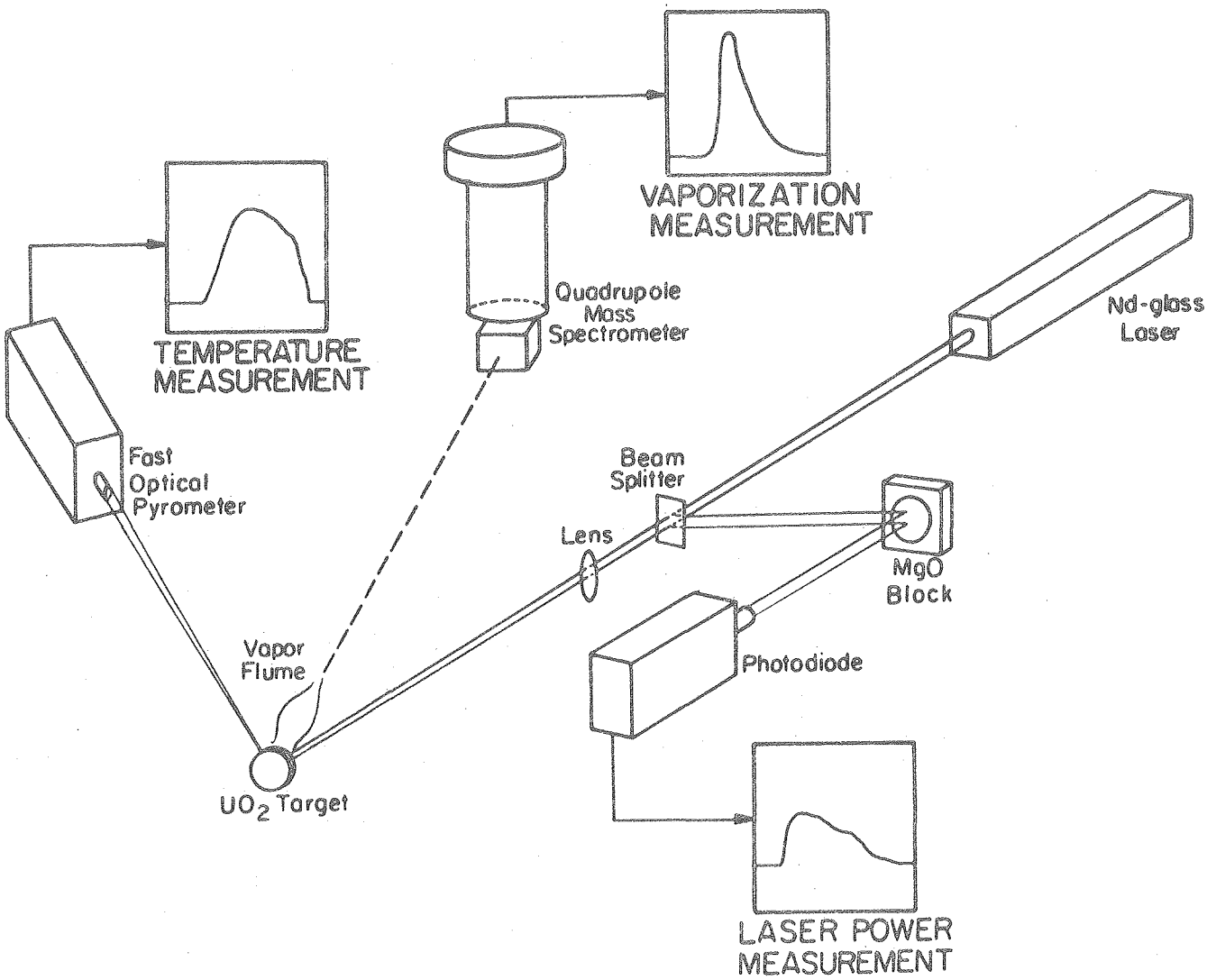

Fig. 7. The experimental apparatus for mass spectrometry measurement at LBL.

Other features of the LBL apparatus are:

(a) The surface temperature is measured by single wavelength (0.65 μm) fast optical pyrometer, which may reduce the optical absorption effect associated with the wide-band optical pyrometer used in the NASA Ames apparatus.

(b) A knife-edge technique has been designed to measure the radial intensity profile of the laser beam to provide the basis for a more accurate temperature calculation.

(c) The target is mounted in an electrom-beam bombardment heater to preheat the target in order to i) avoid in-depth heating by laser penetration by placing the temperature-dependent absorption cut-off of UO_2 at a high wavelength than that of the laser (1.06 μm) (19), and ii) provide steady state calibration signals from the mass spectrometer and the pyrometer prior to each laser pulse.

(d) In order to compare the experimental temperature measurement and theoretical calculation, tungsten and graphite will be studied to take the advantages of well-known high temperature properties of both materials.

(e) In a separate experiment, an array of small disks will be placed around the target spot to collect part of the UO_2 vaporized by a series of laser pulses, as shown in Fig. 8.

The purposes of the device are:

(i) To determine the angular distribution of the vaporized UO_2 by neutron activation of the disks and counting the fission product radioactivity.

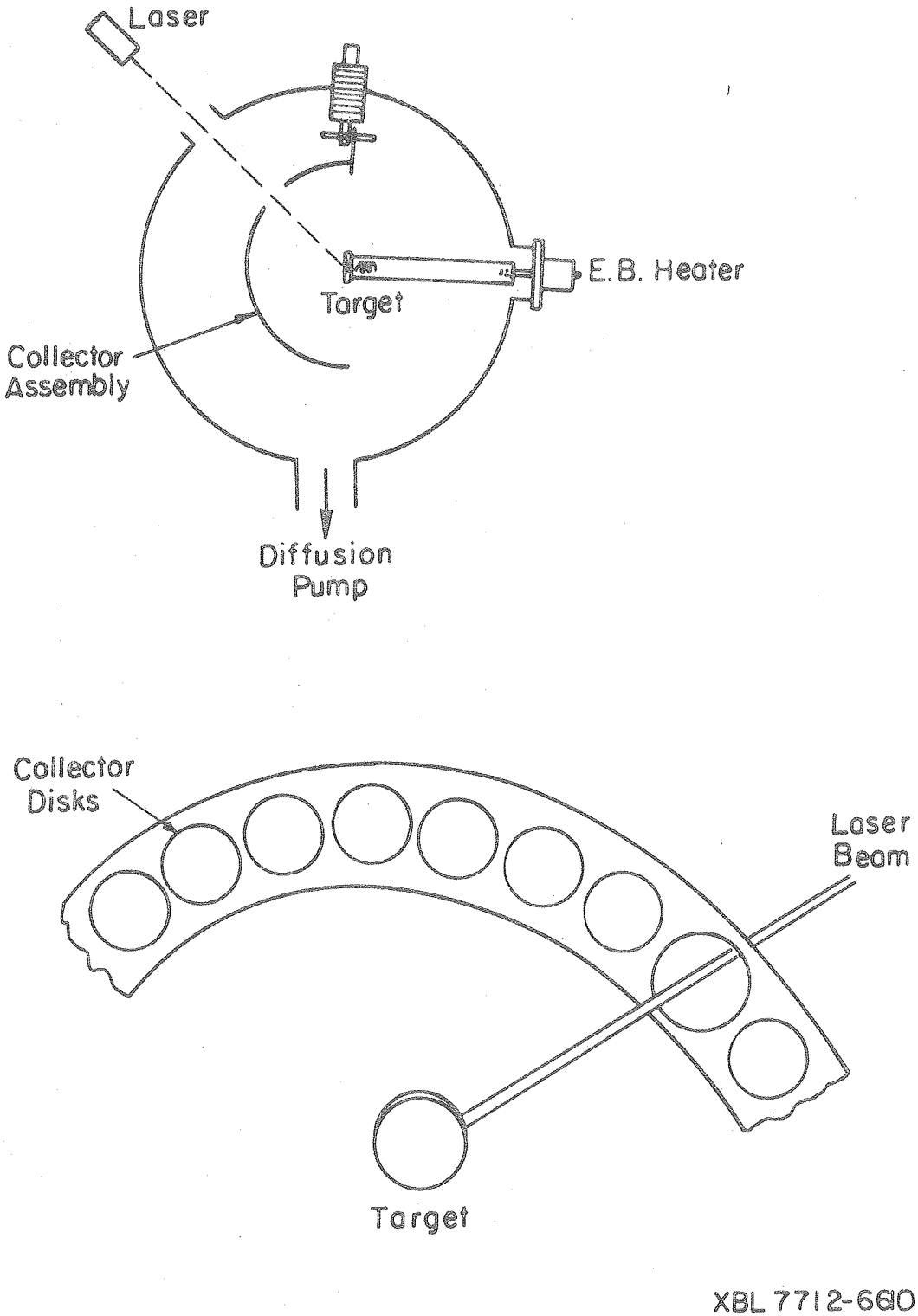

Fig. 8. The collector assembly for angular distribution measurement in LBL's apparatus.

(ii) By integration of the angular distribution over the hemisphere, to provide an independent estimate of the total amount of UO_2 vaporized. This information is difficult to obtain from the mass spectrometer data.

(iii) The UO_2 deposited on the collector disks will be examined by scanning electron microscope for evidence of liquid-droplet mode of ejection from the hot target, or due to condensation in the continuum part of the vapor plume.

(f) A Faraday-cup ion detector assembly has been designed to determine whether the interaction of incident laser beam with the vapor plume or with the solid results in production or emission of ions rather than neutral molecules.

References

1. M.G. Chasanov, L. Leibowitz and S.D. Gabelnick, J. Nucl. Mater. 49, 129 (1973).

2. D.C. Menzies, UKAEA Report TRG-1159 (D) (1966).

3. G.T. Reedy and M.G. Chasanov, J. Nucl. Mater. 42, 341 (1972).

4. R.W. Ohse, P.G. Barrie, H.G. Bogensberger and E.A. Fischer, J. Nucl. Mater. 59, 112: (1976) KFK-2272 (1976).

5. W. Breitung, KFK-2091 (1975).

6. D.L. Booth, UKAEA Report TRG-1759 (1968).

7. M. Bober, J.U. Karow and K. Schretzmann, IAEA Symp. on Thermodynamics of Nuclear Materials, Paper IAEA-SM-190/34 Vienna Oct. 1974.

8. M. Bober, W. Breitung, H.U. Karow and K. Schretzmann, J. Nucl. Mater. 60,20 (1976); KFK-2366 (1976).

9. R.W. Ohse, P.G. Berrie, H.G. Bogensberger and E.A. Fischer, IAEA Symp. on Thermodynamics of Nuclear Materials, Paper IAEA-SM-190/8. Vienna Oct. 1974.

10. R.W. Ohse, P.G. Berrie, H.G. Bogensberger and E.A. Fischer, J. Nucl. Mater. 59, 112 (1976): KFK-2272 (1976).

RETENTION AND RELEASE OF WATER BY UO_2 PELLETS

by Arvind K. Srivastava and Donald R. Olander

Freshly sintered UO_2 pellets readily adsorb moisture from the storage atmosphere. Unless precautions are taken to limit moisture uptake between sintering and fuel element fabrication, the adsorbed water can be released at the high temperatures of in-reactor operation and lead to hydriding of zircaloy cladding. Previous measurements of water released from UO_2 pellets involved heating specimens in vacuum and transferring the gas collected to a calibrated volume where gas composition was measured mass spectrometrically (1). However, in these experiments, it is difficult: 1) to discriminate water released by the specimens from tramp water in the vacuum system, and 2) to avoid loss of water vapor by adsorption on transfer lines and apparatus walls. In our experiment, the first problem is eliminated by adsorbing D_2O on the specimens rather than H_2O and the second difficulty is avoided by in situ mass spectrometry using a modulated molecular beam sampling technique and by maintaining all surfaces >150°C.

As-received UO_2 pellets were given a preliminary anneal in vacuum at 1900°C for 4 hrs. The specimens were quickly transferred to a chamber containing saturated D_2O vapor at room temperature, where they remained for ~2 days. Then, loosely bound physically adsorbed D_2O was removed from the pellets by a week-long dry-nitrogen flush. Following these preparative procedures, 17 g of pellets were loaded into a platinum crucible in the vacuum furnace shown in Fig. 1. D_2O release was monitored in a series of constant-temperature anneals starting at 600°C and proceeding in ~200°C intervals to 1600°C. The hold time at each temperature varied from a few hours to 40 hrs. The experiment lasted 190 hrs, and when it was terminated (by crucible failure), not all of the D_2O had been outgassed.

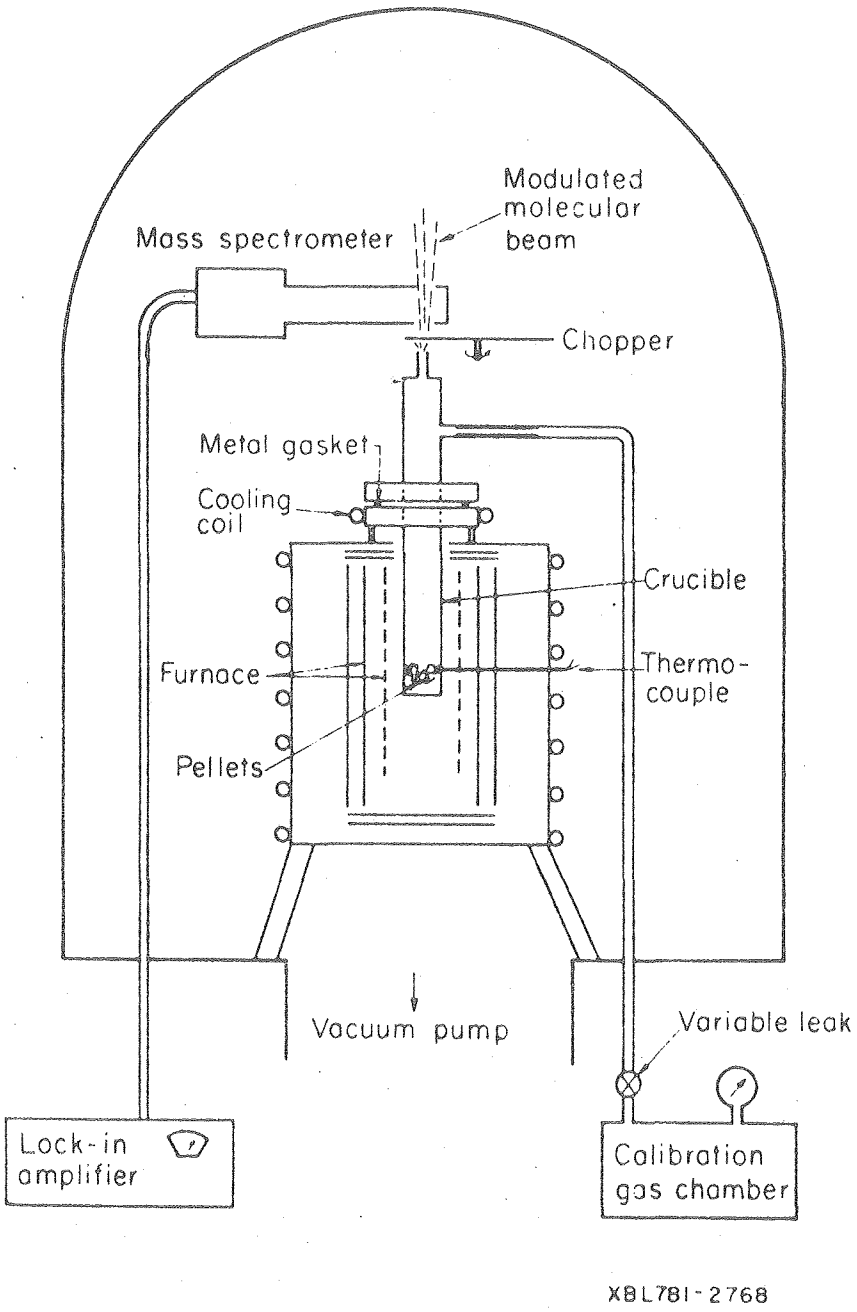

Fig. 1. Apparatus for measuring release of D_2O from UO_2 specimens.

The D_2O released from the sample left the crucible assembly via the upper sampling tube in Fig. 1. The gaseous efflux from this tube was mechanically modulated (chopped) by a rotating toothed disk, so that a modulated, collision-free beam of molecules passed directly through the ionizer of the mass spectrometer. By use of standard phase-sensitive detection methods, only the modulated portion of the mass spectrometer signal was detected, thereby insuring that the D_2O measured came directly from the pellets in the crucible. Absolute release rates were determined by calibrating the system with neon, which was periodically flowed through the assembly at a known rate. The sensitivity of the system was found to be ~1 picogram/sec, which is considerably better than any previous technique.

About 0.6 μg D_2O/g UO_2 were released in the ~4 hrs of outgassing at temperatures below 1000°C. Between 1000 and 1600°C, 12 μg D_2O/g UO_2 were released. This quantity of moisture is larger than that observed in previous investigations (1), which is probably due to the saturated-vapor atmosphere used in our experiments to introduce D_2O into the specimens. In addition, we found that the D_2O was released principally at high temperature, and even here the rates were low. Moreover, the 12 μg/g UO_2 adsorbed is far too large to be distributed as a monolayer on the pellet internal porosity determined by the BET method (~20 cm^2/g UO_2). In fact, the quantity of released D_2O is sufficient to saturate all grain boundaries in the specimens with a monolayer.

Figure 2 shows the release rates for the constant-temperature anneals at 1000, 1200 and 1420°C. The release rate curves at the two highest temperatures can be decomposed into two classes, a short-term release (S) and a long-term component (L). The other significant feature of the release behavior is the resurgence of D_2O outgassing at a new temperature even though the specimens were apparently exhausted of D_2O at the previous lower

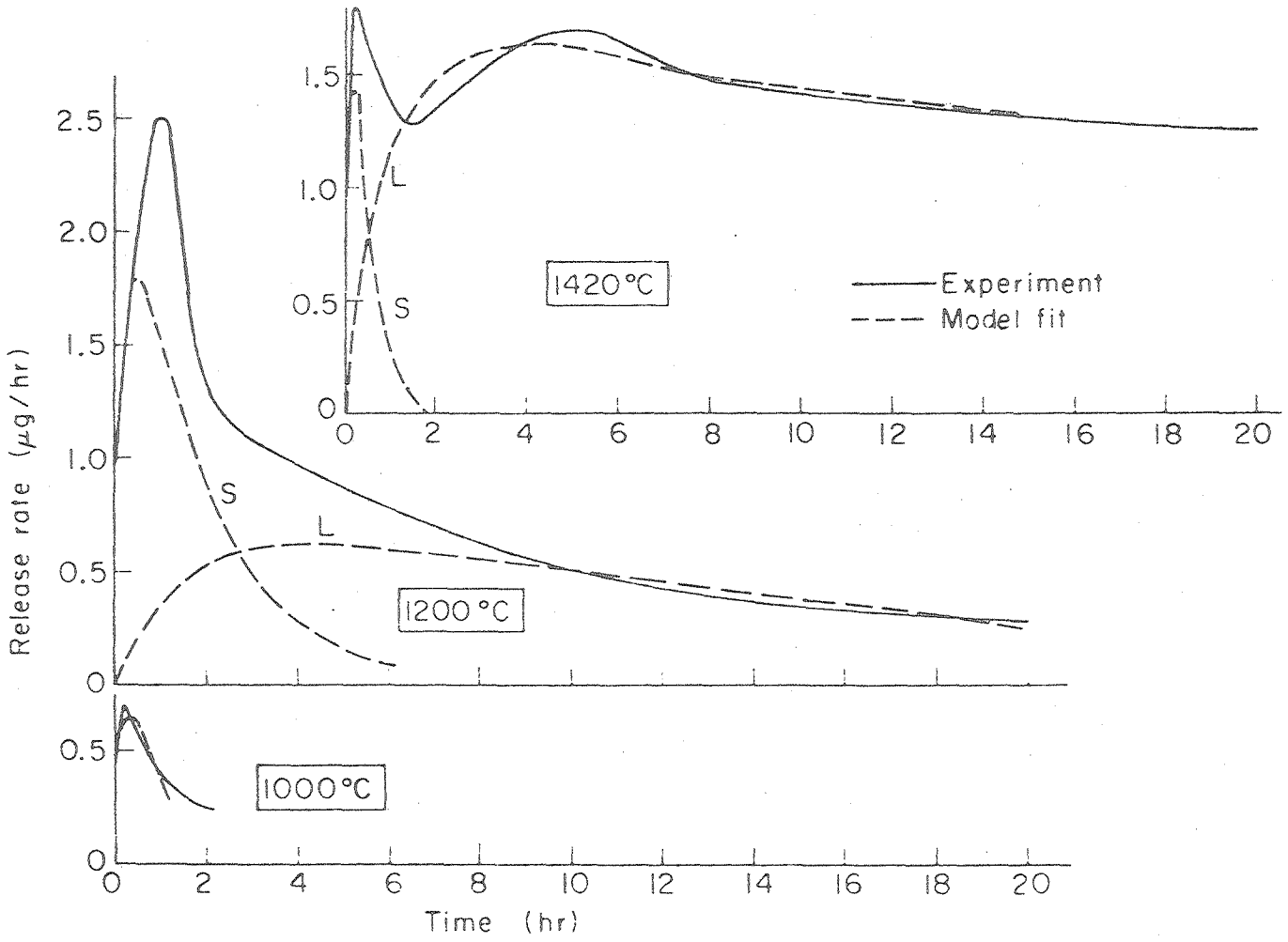

Fig. 2. Rate of release of D_2O from UO_2 at several temperatures.

temperature anneal. This behavior is explained by a multiplicity of binding sites for D_2O on internal surfaces, each characterized by a different binding energy. The dashed lines in Fig. 2 are best-fits of the data to a two-step release model, consisting first of desorption from internal surfaces at a rate determined by the binding energy and followed by permeation (via pores or grain boundaries) to the external vacuum. The data can be fit quite well by this simple model, and the binding energies of each type of adsorption site and the fraction of the total D_2O adsorbed on the site can be determined. Despite the good fit to the data, the model produces binding energies of D_2O to UO_2 which are too large (400-600 kJ/mole). This failing is probably due to neglect of spatial gradients of the D_2O concentration during release and to assuming that desorption is irreversible. The release rates should be analyzed by the diffusion trapping model used to explain fission gas release from irradiated fuels (2). Although this improvement increases the number of parameters to be fit to the data, it provides a better physical description of the water release mechanism.

References

1. C.E.Beyer and C.R.Hahn, BNWL-1956 (1976).

2. D.R.Olander, "Fundamental aspects of nuclear reactor fuel elements," Section 15.6, (ERDA, 1976).

SOLUBILITY OF HYDROGEN IN URANIUM DIOXIDE

by Douglas Sherman

I. INTRODUCTION

When heated to high temperature, UO_2 fuel rods have been found to release hydrogen-bearing gases which may attack the zircaloy cladding. One possible source of hydrogen (other than adsorbed H_2O) is hydrogen dissolved in the lattice of the solid. At present no reliable information on hydrogen solubility in UO_2 is available. Previous results by Wheeler (1) with single-crystal UO_2 produced solubilities ranging from 0.03 to 0.4 micrograms of H_2/g UO_2 with no reproducibility and no apparent pressure dependence. In addition, there is need for knowledge of tritium solubility and permeability in UO_2 for spent fuel reprocessing (2) and in oxides such as Al_2O_3 for assessing the efficacy of coatings on components of a fusion reactor (3).

The three objectives of this project are: (a) to determine the solubility of hydrogen in the lattice of single-crystal UO_2, (b) to determine the chemical nature and location in the microstructure of hydrogen bound in single-crystal and polycrystalline UO_2, and (c) to examine the characteristics of the kinetics of release of hydrogen from single-crystal and polycrystalline samples of UO_2.

II. EXPERIMENTAL

To determine the solubility of hydrogen in uranium dioxide it is necessary to infuse samples with deuterium at high temperature and pressure. The use of deuterium allows the exclusion of any hydrogen background which could be present. The infusion furnace shown in Fig. 1 has been constructed. Basically, it consists of a suspension rig for holding up to 10 grams of solid oxide inside a tungsten susceptor which is heated inductively. This assembly is located inside a 3/8-inch-thick stainless steel pressure vessel. The furnace is capable of attaining 1850°C at 100 atm pressure.

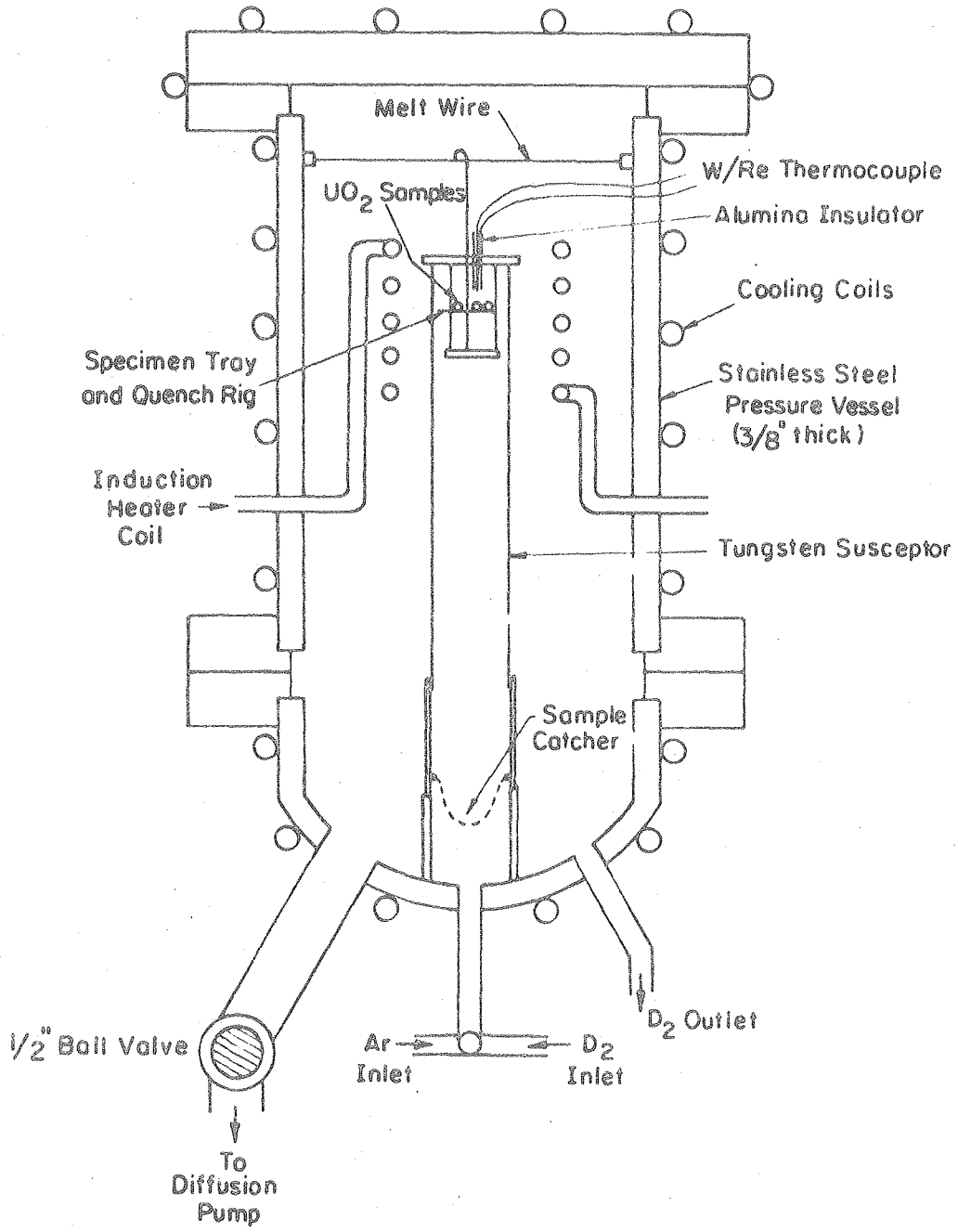

Fig. 1. High pressure furnace for infusing deuterium into solids.

Pressure Vessel

In December of 1976 welding was completed on the pressure vessel. It then underwent an acoustic emission test at the Lawrence Livermore Laboratory up to pressures of 2250 psig, 50% higher than the highest planned experimental pressure. No appreciable leaks were detected; subsequently the ball valve failed because of the low pressure capability of the teflon seat, and was replaced with a delrin seat. The vessel was successfully re-tested at 1900 psi with water by the Mechanical Shop of the Nuclear Engineering Department. In April of 1977 the furnace was mounted on a stand and connected to a 2-inch diffusion pump. Cooling coils were brazed to the pressure vessel and an induction-heater coil was installed.

Sample Heating

The furnace is controlled to give a desired operating temperature by sending the thermocouple output signal to a saturable core reactor which controls the power supply of the induction heater. Due to the problem of electrically insulating the thermocouple from the tungsten susceptor, it was decided to set the maximum operating temperature of the system at 1850°C to permit the use of high-purity alumina insulating tubes. With a W/3% Re-W/25% Re thermocouple in place, the furnace was tested at a temperature of 1000°C under argon.

Sample Manipulation

UO_2 single crystal specimens were obtained from Battelle Pacific Northwest Laboratories in the form of boules from which single crystal specimens can be chipped. The polycrystalline samples in the form of pellets are obtained from Exxon Nuclear Company and the General Electric Company.

A specimen holder for the single crystal samples (~1 gram) as well

as the means for dropping the samples has been constructed and will soon undergo testing. Because of the high diffusivity of hydrogen in UO_2 (1), the infused specimens must be quenched very rapidly in order to preserve the saturation hydrogen content established at the temperature and pressure of the infusion process. The samples are held on an iridium tray suspended by wires. The rig can be quickly tipped by melting a thin wire to which one of the suspension wires is attached (see Fig. 1). The specimens then fall by gravity through the cool D_2 in the lower part of the susceptor tube. Rapid cooling occurs, primarily limited by conduction/convection in the gas surrounding the falling solid. Heat transfer and diffusion calculations have been performed to estimate the quantity of D_2 released (or adsorbed) during the quench. The alteration of the equilibrium content of the solid is not insignificant, but should be less than 25% of the initial amount of dissolved gas. Analytical corrections can be made for this effect. The quenched specimens fall into the catcher mesh at the bottom of the susceptor tube. After the furnace has cooled, it is opened at the top flange and the D_2-saturated specimens are removed for determination of the quantity of dissolved D_2 in the release apparatus described below.

Gas Handling

A flow diagram of the infusion system is shown in Fig. 2. The experimental program calls for infusion gas of either high-purity D_2 or D_2 saturated with D_2O. The first case will use D_2 passed through a liquid nitrogen trap, and for the second, D_2 will pass through a D_2O saturator at 100°C. Everything but the D_2O saturator has been constructed and assembled in place. The construction of the saturator will begin soon. The system was pressurized to 1500 psi of argon in July 1977 and was found to have no appreciable leaks. High temperature and high pressure interlocks for the

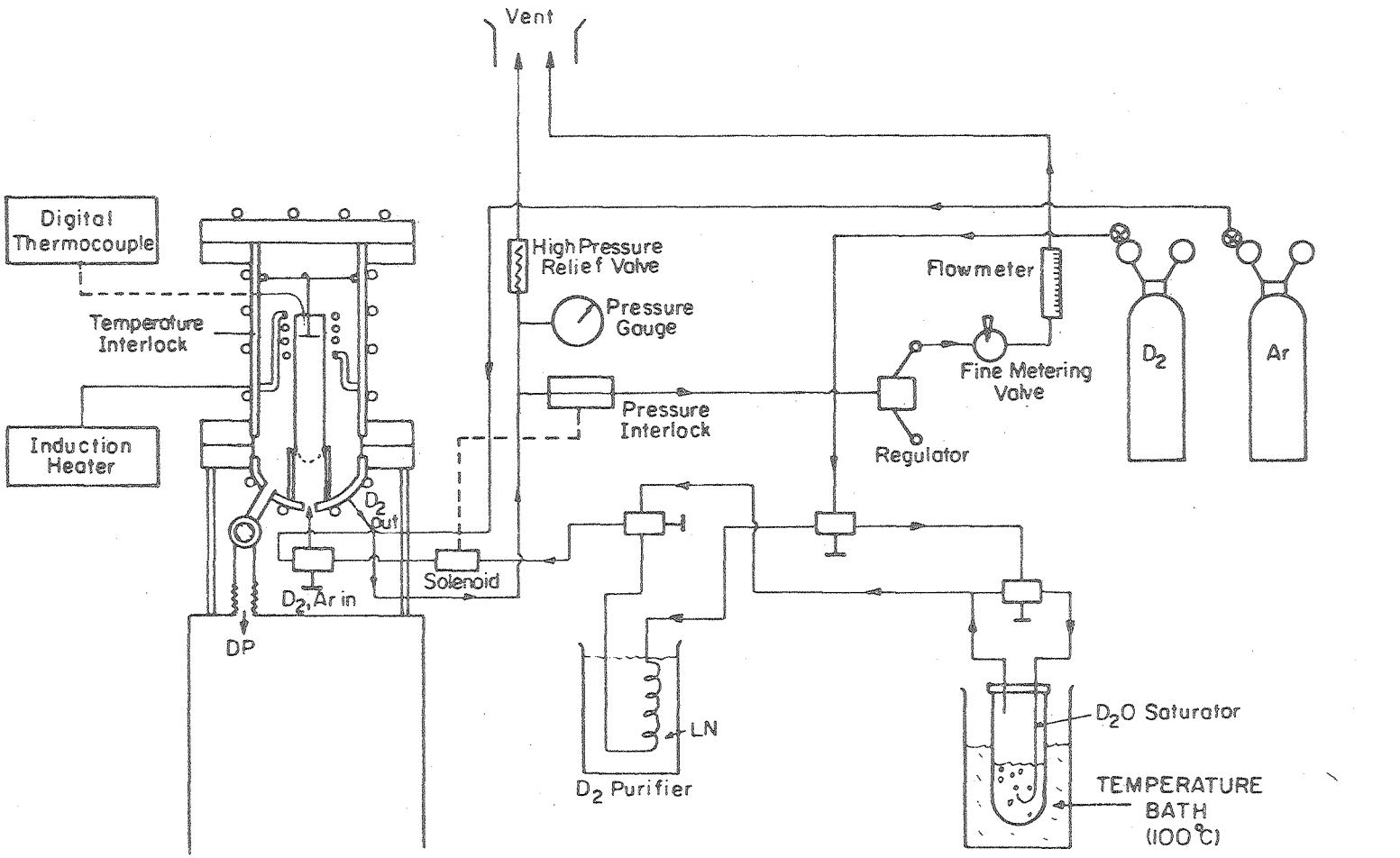

Fig. 2. Flow chart of the gas handling system associated with the infusion furnace.

the system have been installed and tested. Testing with a flow of argon at 2500 cc(STP)/min through the system under experimental conditions is now in progress.

Gas Release Apparatus

The release of deuterium introduced in the samples by the infusion step is to be studied using the apparatus shown in Fig. 3. In order to preserve the D_2O/D_2 ratio of the released gases, the infused samples are heated in a rhenium crucible which is brazed to a molybdenum flange. Release experiments can be conducted at temperatures up to 1850°C. A mass spectrometer is used to monitor the release of D_2, D_2O, and HDO. The latter may result from oxidation of the D_2 by the fuel during the release process.

III. PLANNED EXPERIMENTS

It is not known whether hydrogen dissolves in UO_2 in the form of molecules (Henry's law) or as atoms (Sievert's law). This important feature of the dissolution process will be determined by varying the pressures of D_2 in the infusion step at a fixed temperature and measuring the corresponding solubilities. It is also not known whether hydrogen dissolves in interstitial sites or in anion vacancy sites in the UO_2 lattice. This aspect of hydrogen dissolution will be determined by examining two extremes of urania stoichiometry: UO_{2-x} at the lower phase boundary achieved by infusion in pure D_2, and stoichiometric UO_2 obtained by using an infusion gas with a D_2O/D_2 ratio of ~0.01.

In addition to single crystals, it is planned to conduct similar experiments on hydrogen trapping and release from polycrystalline UO_2. This will enable a determination of the effect of grain boundaries and residual porosity on hydrogen retention in UO_2. Deuterium will be infused

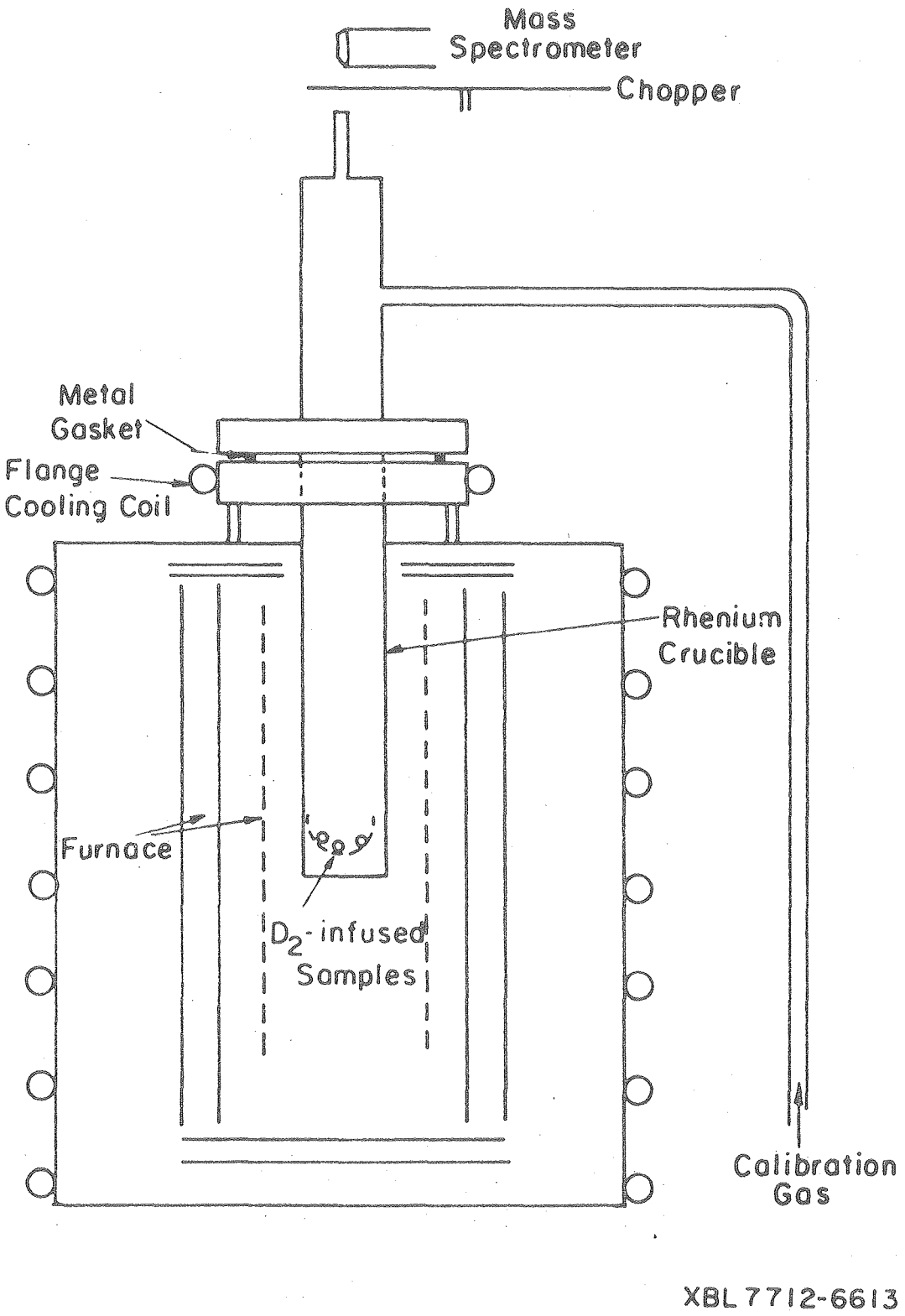

Fig. 3. Vacuum outgassing apparatus for measuring the solubility of deuterium in ceramic oxides.

in these samples and their release subsequently monitored in the same equipment used for the single crystal studies.

References

1. V.J.Wheeler, J. Nucl. Mater. 40, 189-194 (1971).

2. J.H.Goode, ORNL-TM-3273 (1973).

3. T.D.Fowler et al., J. Amer. Cer. Soc. 60, 155 (1977).